IEEE Access
Multidisciplinary ⋮ Rapid Review ⋮ Open Access Journal

Received 18 October 2023, accepted 9 November 2023, date of publication 15 November 2023,
date of current version 21 November 2023.

*Digital Object Identifier 10.1109/ACCESS.2023.3332904*

RESEARCH ARTICLE

# Optimal Scheduling of Electric Vehicle Integrated Energy Station Using a Novel Many-Objective Stochastic Competitive Optimization Algorithm

**BANGLI YIN, XIANG LIAO, BEIBEI QIAN, JUN MA, AND RUNJIE LEI**

Hubei Key Laboratory for High-Efficiency Utilization of Solar Energy and Operation Control of Energy Storage System, School of Electrical and Electronic Engineering, Hubei University of Technology, Wuhan 430068, China

Corresponding author: Xiang Liao (liaoxiang@hbut.edu.cn)

This work was supported in part by the National Natural Science Foundation of China under Grant 51809097, in part by the Open Foundation of Hubei Key Laboratory for High-Efficiency Utilization of Solar Energy and Operation Control of Energy Storage System under Grant HBSEES202312, and in part by the Open Foundation of Hubei Engineering Research Center for Safety Monitoring of New Energy and Power Grid Equipment under Grant HBSKF202125.

**ABSTRACT** The construction of the Electric Vehicle Integrated Energy Station (EV-IES) is a prerequisite for the rapid development of the EV industry. However, how to optimize the operation of the EV-IES is a problem worthy of study. Therefore, this paper designs an EV-IES model with PV and Energy Storage System (ESS). Fully consider the peak-valley time-of-use electricity price, user traffic flow, PV output, and other factors. On this basis, the three objectives of the maximum daily revenue of the EV-IES, the minimum exchanged energy between the EV-IES and the Regional Power System (RPS), and the minimum pollutant emission are optimized at the same time. Secondly, this paper proposes a Many-objective Stochastic Competition Optimization (MOSCO) algorithm, which is utilized to assess the DTLZ1-7 benchmark functions and the optimization scheduling problem of EV-IES. By comparing its simulation results with those of five other optimization algorithms, it is evident that the MOSCO algorithm outperforms the other five in terms of IGD, GD, HV, and Spread values. This indicates the effectiveness of the MOSCO algorithm in addressing many-objective optimization problems. Finally, in order to illustrate the feasibility of designing the EV-IES model, three comparative cases were designed. The Pareto solutions of these cases were obtained using the MOSCO algorithm, and the Entropy-Technique for Order Preference by Similarity to Ideal Solution (ETOPSIS) method was applied to determine the optimal solution for each case. Compared to the traditional charging station (case 1), the daily revenue of the EV-IES increased by 27.97%. Pollutant emissions were reduced by 25.29%.

**INDEX TERMS** Electric vehicle, EV integrated energy station, many-objective optimal scheduling, MOCSO algorithm.

## NOMENCLATURE

| | |
|---|---|
| ANSGA-III | Adaptive-reference-point-based Nondominated Sorting Genetic Algorithm. |
| BWO | Black Widow Optimization. |
| EV | Electric Vehicle. |
| ESS | Energy Storage System. |
| EV-IES | Electric Vehicle Integrated Energy Station. |
| ETOPSIS | Entropy-Technique for Order Preference by Similarity to Ideal Solution. |
| MOSCO | Many-objective Stochastic Competition Optimization. |
| MOPSO | Multi-objective Particle Swarm Optimization. |
| NSGA-II | Non-dominated Sorting Genetic Algorithm II. |
| NSGA-III | Non-dominated Sorting Genetic Algorithm III. |
| NIS | Negative Ideal Solution. |
| PV | Photovoltaic. |
| EDNSGA-II | Economic Dispatch based Non-dominated Sorting Genetic Algorithm II. |

The associate editor coordinating the review of this manuscript and approving it for publication was Amin Mahmoudi.

| | |
|---|---|
| FCSS | Fast Charging Service Station. |
| GA | Genetic Algorithm. |
| GLMO | Grouped and Linked Mutation Operator. |
| HESS | Home Energy Storage System. |
| MGSOACC | Multi-objective Group Search Optimizer with Adaptive Covariance matrix and Chaotic search. |
| PIS | Positive Ideal Solution. |
| PSO | Particle Swarm Optimization. |
| RPS | Regional Power System. |
| SOC | State Of Charge. |
| SO | Snake Optimization. |
| t-DEA | Theta Dominance based Evolutionary Algorithm. |

## I. INTRODUCTION

In recent years, the world has advocated efficient, clean, and sustainable energy development. Traditional fuel engine vehicles have the disadvantages of high carbon emissions and high energy consumption [1]. At the same time, with China setting dual carbon goals, electric vehicles play a crucial role in achieving these objectives [2], [3]. Therefore, the electric vehicle industry is in the development stage, and it is expected that electric vehicles will grow exponentially in the next few years.

Several studies have addressed optimal charging schedules for Electric Vehicles (EVs). Li et al. [4] propose a charge-discharge strategy that can be automatically adjusted to the change in time-varying peak-to-valley tariffs. Kang et al. [5] propose a centralized charging strategy for EVs in a battery-switching scenario. Zhao et al. [6] developed an optimization model that incorporates wind and solar energy, energy storage systems, gas turbines, and the regional power system. Reference [7] propose a smart charging strategy to avoid EV charging hours overlapping with residential peak load hours. Reduces grid power losses and voltage deviations while satisfying EV charging services [8]. Li et al. [9] established a model for electric vehicle swapping stations, which primarily consists of electric vehicles and the regional power system. They formulated an objective function to minimize battery acquisition costs and addressed the battery capacity decision problem. Additionally, they proposed a centralized optimization scheduling strategy. In this paper, according to the peak-valley time-of-use price of the Regional Power System (RPS), EV charging load of the Fast Charging Service Station (FCSS), and photovoltaic (PV) output, the charging and discharging amount of Energy Storage System (ESS) in each period is determined.

At present, there is both single-objective and many-objective optimization research on the optimal scheduling of Electric Vehicle Integrated Energy Station (EV-IES). The incorporation of EVs into an integrated energy system can serve as a cornerstone of a decarbonized economy while also lowering the long-term cost of an integrated energy system [10]. Document [11] proposes a home energy management system composed of solar energy, a Home Energy Storage System (HESS), and an EV. This system optimizes the peak load of RPS by scheduling the charge and discharge strategies of the EV and HESS Baik et al. [12] propose a method to calculate the specific number of EV charging equipment and the capacity of auxiliary equipment for fast charging station operators to maximize the revenue of the fast charging station. In [5], a centralized charging strategy is proposed to reduce the overall charging cost and to centrally charge batteries during peak hours of the grid. Zaher et al. [13] constructed the model of the exchange station to determine the best charge-discharge and exchange plan for the battery of the swapping station to reach the maximum economic revenue. Wind energy and solar energy have the characteristics of uncertainty and intermittency. Therefore, in the optimization scheduling of EV-IES with wind and solar systems, ESS are essential components [14]. Zhao et al. [15] developed a battery charging and swapping station model that incorporates changes in State of Charge (SOC) and includes wind and solar energy, energy storage systems, and the power grid. They simultaneously optimized three objectives: transmission losses, voltage deviations, and wind and solar energy curtailment. Furthermore, they employed a many-objective weighted method to transform the many-objective optimization problem into a single-objective optimization problem. In the context of the existing single-objective study, the optimization objectives are basically in-station economic benefit, charging cost, life cycle cost [16], grid load variance, etc.

After reading the recent literature, it is not difficult to find the application of many-objective optimization to EVs and smart grids. A dynamic prediction method is proposed in [17] to determine the optimal location and capacity of the EV charging station. Yao et al. [18] balanced the conflicting objectives of minimizing annual investment and total energy cost and maximizing annual angular flow to increase the economic return to the investor. However, the optimal charging schedule for individual EV users is not addressed, affecting EV user satisfaction. In [19], a model of fast EV charging stations for wind, PV, and storage systems is constructed to minimize the cost of electricity and environmental pollution emissions. The model is solved using a Multi-objective Particle Swarm Optimization (MOPSO) algorithm to determine the optimal capacity of each system. This study takes into account the economic and environmental aspects of the fast charge station but does not consider the potential interference between the fast charge station and the RPS. Wang et al. [20] studied EV travel law and constructed a regional electricity price optimization model to maximize the economic benefits of charging stations and minimize regional load peaks. Although this study examines the impact of charging stations on the RPS, it does not address environmental objectives to reduce pollutant emissions. Li et al. [21] integrated a PV power generation system into a centralized battery replacement charging system, proposed a centralized battery replacement charging system to minimize the total operating

**TABLE 1. The above research explores the differences among various optimization scheduling models.**

| References | Components | Objectives | Method |
|---|---|---|---|
| [5] | EVs and RPS | Charging cost, power loss, and voltage deviations | PSO-GA+ |
| [6] | EVs, PV, Wind, ESS, and gas turbine | Total cost | Linear programming algorithm |
| [7] | EVs and RPS | Total travel time and charging cost | Ant colony optimization |
| [8] | EVs and RPS | Charging Service Ability, power losses, and voltage deviations | Cross-entropy method |
| [9] | EVs, BSS and RPS | Battery purchase cost | GA |
| [10] | PV, Wind, BESS, EVs and RPS | Sustainability Costs | GAMS |
| [11] | PV, EVs, and home battery | Energy cost | Linear programming algorithm |
| [12] | EVs, PV, and BESS | Charging station operator profit | GAMS |
| [13] | EVs and battery exchange stations | Battery exchange stations owner profit | Mixed-integer programming |
| [14] | EVs, PV, Wind, and ESS | Profit of the entire system, Profit of storage/EV owners, and generation output from renewables | Many-objective weighted method |
| [15] | EVs, PV, Wind and RPS | Curtailment percentage of wind and PV power, transmission losses and voltage deviation | Many-objective weighted method |
| [16] | PV, Wind, and load | Total life cycle cost | Hybrid CS-HS-SA algorithm |
| [17] | EVs and RPS | Captured charging demands; total cost of electricity and the time consumed for charging, and load variance of the power grid | Hybrid PSO |
| [18] | EVs and RPS | The overall annual cost of investment and energy losses, the annual captured traffic flow | MOEA/D |
| [19] | PV, Wind, EVs, and BESS | Cost of electricity and pollution emissions | MOPSO |
| [20] | EVs and RPS | Power load and profit | NSGA-II |
| [21] | EVs, BSS, PV and RPS | Total operation cost and smooth load fluctuations | NSGA-II |
| [22] | EVs and RPS | Charge cost and variance of load | NSGA-II |
| [23] | EVs, PV, and RPS | Energy cost, grid net exchange, and $CO_2$ emission | Augmented non-dominated ε-constraint method |
| [24] | EVs, PV, BESS, and RPS | Total profit and BESS capacity fading | Augmented ε-constraint |
| [25] | EVs, PV, ESS, and RPS | Energy costs and carbon transaction costs | Linear programming algorithm |
| Ours | EVs, PV, ESS, and RPS | The daily revenue, the exchanged energy between the RPS and the EV-IES, and the pollutant emissions | MOSCO |

cost with a smooth load fluctuation many-objective optimization operation method, and also proposed a many-objective optimization algorithm that modifies the Non-dominated Sorting Genetic Algorithm III (NSGA-III) cross variance operator to solve the model. However, they propose a method that does not consider the environmental pollution caused by energy originating from the grid side. Wang et al. [22] constructed an interaction model between the distribution network and EVs, developed an orderly charging strategy, and proposed a method to optimize operation with minimum charging cost and load variance. Das et al. [23] study the joint optimal scheduling of EV charging stations, battery replacement stations, and renewable energy. Meanwhile, propose a many-objective technical economic environmental concept of EV charger and discharger scheduling. Constructing four objective functions for user-side energy cost, battery degradation, grid interaction energy, and carbon emission is a typical many-objective optimization problem. However, on the power supply side, the regional power system's power generation process is inevitably accompanied by pollutants other than carbon pollution. Eldeeb et al. [24] proposed an approach to optimize the operation of the PV-EV station to maximize the daily economic benefit of charging stations while reducing the capacity decline of the battery storage system. They studied the battery storage capacity variation, which is also not covered in this paper, but they not only did not consider the impact on the RPS but also did not reduce pollutant emissions. Shi et al. [25] Use a weighted approach to simultaneously optimize energy costs and grid load. Operational carbon emission constraints reduce carbon emissions. However, it is not optimized as a separate objective, and the relationship between the objectives cannot be weighed. Apart from [21], a new many-objective optimization algorithm is not proposed, but the model is solved by applying the existing many-objective algorithm.

Based on the aforementioned research, numerous scholars have made significant contributions to the field of optimal scheduling for EV-IES. It is evident that the optimization and scheduling of EV-IES represent a many-objective optimization problem. In existing studies, most models for EV-IES are predominantly single-objective or bi-objective optimization models, typically solved using solvers, linear programming methods, or artificial intelligence algorithms. Some studies also employ weighted approaches to transform the many-objective optimization problem of EV-IES into a single-objective problem for solving. Additionally, it can be

observed that the economic benefit of EV-IES is a crucial indicator in the optimization models and is considered one of the objective functions in this paper. The objective function involving the exchange energy between the RPS and EV-IES reflects the energy interaction between the two systems in different time periods, reducing the impact on the RPS. As China setting dual carbon goals, pollutant emissions are also considered as one of the objective functions in this paper. Existing literature has not yet addressed the simultaneous optimization of these three objectives in scheduling models. Therefore, this paper aims to optimize all three objectives concurrently. The distinctions between our study and the aforementioned research are summarized in Table 1.

The model-solving method is a crucial part of the optimal scheduling problem for EV-IES. Dominguez-Navarro et al. [26] optimized of the installation and operation of an EV fast charging station using a Genetic Algorithm (GA). Zheng et al. [27] show that the optimal scheduling of an integrated energy system is a non-convex and non-linear optimization problem, as is the problem of optimal scheduling of EV-IES, both of which are many-objective optimization problems. Yao et al. [18] designed an integrated charging system for power distribution and EVs. The Multi-objective Evolutionary Algorithm Based on Decomposition (MOEA/D) optimization algorithm is applied to solve the model to obtain a non-dominated solution. Wei et al. [28] used the life-cycle mean and deviation to evaluate the investment cost and risk of an integrated energy system and proposed a Multi-objective Group Search Optimizer with Adaptive Covariance matrix and Chaotic search (MGSOACC) algorithm to solve this many-objective optimization problem. Miao et al. [29] considered the interests of users on the one hand and service providers on the other. From different perspectives, two conflicting objectives are established, and the Non-dominated Sorting Genetic Algorithm II (NSGA-II) is applied to obtain the Pareto solution. Due to the fact that EV-IES is a many-objective and multi-constraint model, this paper proposes Many-objective Stochastic Competition Optimization (MOSCO) for solving this model.

Since the many-objective optimization algorithm solves the optimization model to obtain a set of Pareto solutions. How to determine the optimal solution from the Pareto solution is a major difficulty faced by decision-makers. Therefore, this paper uses the Entropy-Technique for Order Preference by Similarity to Ideal Solution (ETOPSIS) decision method to determine the optimal solution from the Pareto solution. Xu et al. [30] used the NSGA-II algorithm to solve the many-objective optimization model of the hybrid energy storage system configuration and used the VlseKriterijumska Optimizacija I Kompromisno Resenje (VIKOR) method to determine the optimal solution. Sarshar et al. [31] used the TOPSIS method to find the optimal solution from the Pareto solution of the Economic Dispatch-based Non-dominated Sorting Genetic Algorithm II (EDNSGA-II) algorithm. Sun [19] used the MOPSO algorithm to solve the many-objective fast charging station optimization model and used the TOPSIS method to determine the optimal solution from the Pareto solution.

The contributions of this paper are summarized as follows:

(1) In this paper, a joint optimal scheduling model of EV-IES and RPS, which includes PV, ESS, and FCSS is proposed. The EV-IES model not only meets the charging demand of EV users but also enhances daily economic benefits while reducing pollutant emissions.

(2) At the same time, for the first time, the daily revenue of EV-IES, the energy exchange between RPS and EV-IES, and pollutant emissions have been optimized synchronously.

(3) A new MOSCO algorithm is proposed. It calculates GD and IGD values using DTLZ1-7 benchmark functions and obtains Spread, HV, and Runtime data during model solving. These results are compared with the outcomes of five other algorithms to demonstrate that MOSCO possesses strong solving capabilities and can effectively address high-dimensional many-objective optimization problems.

The rest of this paper is organized as follows. Section II explains the mathematical model of the EV-IES in detail. Section III elaborates on the methods for determining the optimal solution of the EV-IES model. Section IV describes how the decision variables of the model are converted into the energy flow of each system and determines the range of random numbers of the MOSCO algorithm for solving the EV-IES model. Section V shows the simulation results and results analysis; Section VI concludes the paper.

## II. MATHEMATICAL MODEL OF THE EV-IEES

### A. EV-IES

The EV-IES consists of three subsystems: PV system, ESS, and FCSS. At the same time, the station is connected to the RPS. Therefore, the station can purchase or sell electricity from the RPS. The EV-IES not only meets the charge needs of users, but can also use RPS to achieve energy arbitrage, thereby improving the economic benefits of the EV-IES. The overall model is shown in Fig. 1. The whole EV-IES realizes the dynamic interaction of power generation, EV battery charging operations for users, and energy inter-feeding with the RPS. The components of each subsystem of the station are described as follows:

(1) PV system: PV panels are directly connected to the AC bus through the AC/DC module. PV panels convert solar energy into electrical energy; that can be stored in the ESS, used for user EV charging, or grid-connected to the RPS. Its installed capacity is 62.51 kW.

(2) ESS: It consists of 20 EV batteries of 60 kW, which are connected to the AC bus through AC/DC modules. The ESS can not only absorb the power generated by the PV system but also supply power to the EV. In addition, it can regulate the peak and valley values of the RPS load.

(3) Fast charging service station: It consists of 12 charging posts. When EV users arrive at the EV-IES and charge the EV battery to the State of Charge (SOC) limit to meet user demand.

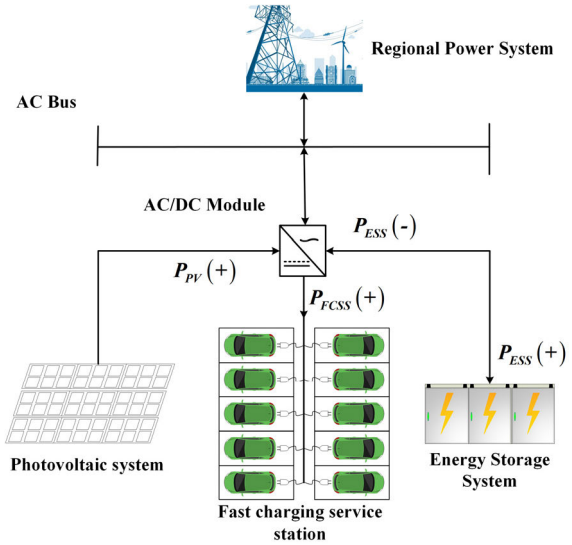


$P_{ESS}(+/-)$:The ESS is capable of bidirectional energy transfer. If the ESS is in a discharge state , $P_{ESS}$ is a negative value, it is represented by $P_{ESS}(+)$. Conversely, if the ESS is in a charge state, $P_{ESS}$ is a Negative Value, it is represented by $P_{ESS}(-)$.

$P_{FCSS}(+)$ :The energy consumed by the FCSS system is actually the EV charging load. In fact, the FCSS can be considered as a load, and there is no energy flow out of it. Therefore, $P_{FCSS}$ values are all positive.

$P_{PV}(+)$ :The PV system generates energy; therefore, the energy flowing out of the photovoltaic system, denoted as $P_{PV}$ , is always positive.

**FIGURE 1. Structure diagram of EV integrated energy station.**

### B. MATHEMATICAL MODEL

The EV-IES designed in this paper is a many-objective optimization model that aims to maximize the daily revenue of the EV-IES, minimize the exchanged energy between the RPS and the EV-IES, and minimize pollutant emissions while satisfying all constraints.

#### 1) OBJECTIVE FUNCTIONS

(1) EV-IES with maximum daily revenue

The daily revenue of the EV-IES is a basic economic indicator, and the main source consists of two parts: (1) The revenue from charging the batteries of EV users by the EV-IES. (2) The ESS charges the RPS during off-peak load periods and feeds power back to the RPS during peak load periods. They form a mutual feedback relationship, and energy arbitrage is realized. Therefore, the objective function of maximizing the daily revenue of the EV-IES can be described as Equation (1).

$$\begin{aligned}\max F1 = &\sum_{t=1}^{24} P_{FCSS}(t) \times \Delta h \times p_{charge} \\ &+ \sum_{t=1}^{24} (P_{ESS}(t) + P_{FCSS}(t) - P_{PV}(t)) \\ &\times \Delta h \times Ce(t) \end{aligned} \tag{1}$$

where $P_{ESS}(t)$ is the charging power of the ESS to the RPS at time t; $P_{PV}(t)$ is the PV output power at time t; $P_{FCSS}(t)$ is the charging power of the FCSS at time t; $p_{ch\arg e}$ is the price of EV charging (where $p_{ch\arg e} = 1.2568$); $Ce(t)$ is the peak-to-valley electricity tariff; $\Delta h$ is the charging time. The calculation method for $P_{PV}(t)$ and $E_{ESS}(t)$ is as follows:

The mathematical model of its PV panel output power can be described as Equation (2) [32].

$$P_{PV}(t) = \frac{G_c(t)}{G_r} \times P_{rp-PV} \times \eta_{PV} \times [1 + k(T_c(t) - T_{rc})] \tag{2}$$

where $G_c(t)$ is the sunlight intensity at time t; $G_r$ is the rated insolation intensity in a standard scenario (the standard insolation intensity in this paper is 1000 W/m$^2$); $P_{rp-PV}$ is the rated power of PV panels at standard temperature and sunlight intensity (25 kW); $\eta_{PV}$ is the efficiency of PV panels to generate electricity (85%); $T_c(t)$ is the temperature at time t; $T_{rc}$ is the rated temperature in a standard scenario (the temperature is 25°$C$); $k$ is the power temperature coefficient.

The mathematical model of its ESS can be described by Equation (3).

$$\begin{aligned}E_{ESS}(t) = E_{ESS}(t-1) + [&P_{ESS}^{ch\arg e}(t) \times \eta_{ESS}^{ch\arg e} \times \mu_{ESS}^{ch\arg e} \\ &- P_{ESS}^{disch\arg e}(t)/\eta_{ESS}^{disch\arg e} \times \mu_{ESS}^{dischage}] \times \Delta h \end{aligned} \tag{3}$$

where $E_{ESS}(t)$ is the amount of electricity in the ESS at time t; $P_{ESS}^{ch\arg e}(t)$ and $P_{ESS}^{disch\arg e}(t)$ are the charging and discharging power of the ESS at time t, respectively; $\mu_{ESS}^{ch\arg e}$ and $\mu_{ESS}^{disch\arg e}$ are binary numbers that indicate the discharging and charging states of the ESS, respectively $\eta_{ESS}^{ch\arg e}$ and $\eta_{ESS}^{disch\arg e}$ represent the charging and discharging efficiency of the ESS, respectively.

(2) Minimization of exchanged energy between the RPS and the EV-IES

The ESS of the EV-IES discharges during the peak load of the RPS and charges otherwise. In this way, the load curve of the RPS becomes flat and the peak-to-valley difference becomes smaller, which makes the RPS operate more safely. Therefore, the objective function of the energy exchange between the RPS and the EV-IES can be described as Equation (4).

$$\min F2 = \sqrt{\sum_{t=1}^{24} (P_{ESS}(t) + P_{FCSS}(t) - P_{PV}(t))^2} \tag{4}$$

(3) Minimal pollutant emissions

EVs are considered the main solution to reduce pollutant emissions in the global transportation sector. In EV-IES, the main source of environmental pollutants is the portion of electricity purchased from the RPS. Therefore, the pollutant emission minimization model is intended to reduce emissions of $CO_2$, $SO_2$, and $NO_x$. The objective function of pollutant emissions can be described as Equation (5)-(6) [19].

$$\min F3 = \sum_{t=1}^{24} P_{Grid}(t) \times \Delta h \times (e_{CO_2} + e_{SO_2} + e_{NO_x}) \tag{5}$$

$$P_{Grid}(t) = \begin{cases} 0 & P_{ESS}(t) + P_{FCSS}(t) \le 0 \\ P_{ESS}(t) + P_{FCSS}(t) & P_{ESS}(t) + P_{FCSS}(t) > 0 \end{cases} \tag{6}$$

where $e_{CO_2}, e_{SO_2}, e_{NO_x}$ is the emission factor of $CO_2$, $SO_2$, $NO_x$ respectively $P_{Grid}(t)$ is the power charged from the RPS to the EV-IES at time t; In [19] $e_{CO_2} = 0.997kg/kWh$, $e_{SO_2} = 0.03kg/kWh$, $e_{NO_x} = 0.015kg/kWh$.

### 2) CONSTRAINTS

(1) Equation (7) is the power constraint equation for ESS charging in each time period.

$$P_{ESS}(t) = N_B \times B_{Cap} \times (SOC(t) - SOC(t-1)),\ t = 1, 2, \ldots, 24 \tag{7}$$

where $N_B$ is the number of ESS batteries; $B_{Cap}$ is the rated capacity of the EV battery; $SOC(t)$ is the state of charge of the ESS at time t.

(2) Equation (8) represents the energy balance of various subsystems within the EV-IES model.

$$(P_{ESS}(t) + P_{PV}(t) + P_{FCSS}(t) + P_{RPS}(t)) \times \Delta h = 0 \tag{8}$$

where $P_{RPS}(t)$ the power supplied by RPS to the EV-IES model.

(3) Equation (9) is the priority of each system charging.

$$P_{FCSS} \triangleleft \{P_{RPS}, P_{ESS}\} \tag{9}$$

where $A \triangleleft B$ represents that A is superior to B, $\triangleleft$ is the priority symbol.

(4) Equation (10)-(11) is the constraint on the battery SOC.

$$SOC_{\min} \le SOC(t) \le SOC_{\max} \tag{10}$$

$$SOC^{ESS}(0) = SOC^{ESS}(24) = 20\% \tag{11}$$

where $SOC_{\min}$ is the lower limit of the battery state of charge, which is taken as 20% in the paper; $SOC_{\max}$ is the upper limit of the battery state of charge, which is taken as 80% in the paper; $SOC^{ESS}(0)$ is the starting charge state of the ESS; $SOC^{ESS}(24)$ is the termination of the ESS charge state.

(6) Equation (12)-(13) is the constraint on charging and discharging power.

$$0 \le |P_{ESS}(t)| \le P_{\max} \tag{12}$$

$$0 \le |P_{FCSS}(t)| \le N_B \times P_{FCSS}^{\max} \tag{13}$$

where $P_{\max}$ is the maximum charging power of the ESS; $P_{FCSS}^{\max}$ is the maximum charging power of the charging post at the FCSS.

(6) Equation (14) is the constraint on the ESS capacity.

$$E_{ESS}^{\min} \le E_{ESS}(t) \le E_{ESS}^{\max} \tag{14}$$

where $E_{ESS}^{\min}$ is the minimum allowable storage capacity of the ESS; $E_{ESS}^{\max}$ is the maximum allowable storage capacity of the ESS.

(7) Equation (15) is the constraint for the balance between charging and discharging of the ESS.

$$\sum_{t=1}^{24} P_{ESS}(t) \times \Delta h = 0 \tag{15}$$

(8) Equation (16) is the constraint for ESS charging and discharging operations.

$$\mu_{ESS}^{disch\arg e} \times \mu_{ESS}^{ch\arg e} = 0 \tag{16}$$

## III. METHODOLOGY

In order to obtain the optimal solution of the EV-IES optimization model, this paper proposes a MOSCO algorithm. The MOSCO algorithm is used to solve the optimization model to obtain the Pareto solution, and then the ETOPSIS method is applied to determine the optimal solution of the optimization model. The solving process of the EV-IES optimization model is shown in Fig. 2.

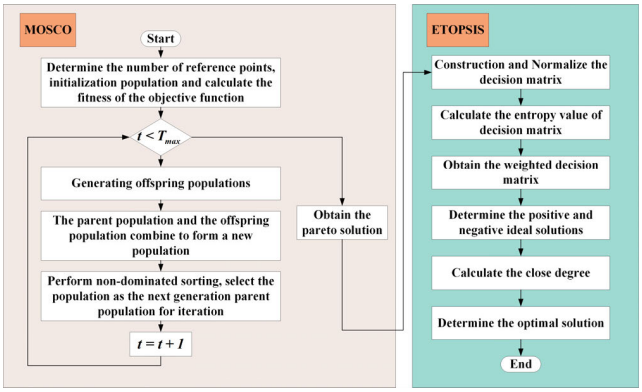


**FIGURE 2.** The solving process of the EV-IES optimization model.

### A. MOSCO ALGORITHM

Due to the optimization problem of EV-IES is a multi-constraint and many-objective problem. Therefore, the algorithm for solving the EV-IES model needs to have stronger search and convergence capabilities. Because the Black Widow Optimization (BWO) algorithm [33] and Snake Optimization (SO) algorithm [34] have good global search ability and convergence ability. The Levy strategy can effectively prevent the algorithm from falling into local optimum. Therefore, the MOSCO algorithm draws on the BWO algorithm pheromone update method and the SO global search method and introduces the Levy strategy. Its pseudo-code is shown in Algorithm 1.

The steps of the MOSCO algorithm are as follows:

Step 1: Initializing the parent population $N_t$, the maximum number of iterations $T_{\max}$, and input the initial data of the EV-IES, such as traffic flow, PV output, etc.

Step 2: Generate a random number $r$, and determine the population update method according to the size of the random number.

When $r \leq R_1$, the population update method adopts Equation (17):

$$\vec{X}_i(t+1) = \frac{1}{2}[\vec{X}_{r1} - (-1)^{val}\vec{X}_{r2}] \tag{17}$$

where $\vec{X}_i(t+1)$ is the individuals after the position update; $r_1$ and $r_2$ is the random number in the range $[1, N]$; $val$ is a binary number.

When $r > R_1 \&\& r \leq R_2$, the population update method adopts Equation (18):

$$\vec{X}_i(t+1) = \begin{cases} \vec{X}_{r1} - rand() \times ((upper - lower) \\ \times rand() + lower) \\ \qquad rand() > 0.5 \\ \vec{X}_{r1} + rand() \times ((upper - lower) \\ \times rand() + lower) \\ \qquad rand() \leq 0.5 \end{cases} \tag{18}$$

where $rand()$ is the uniformly distributed random number; $upper$, $lower$ is the upper and lower bounds of the population, respectively.

When $r > R_2$, the population update method adopts Equation (19)-(21):

$$\vec{X}_i(t+1) = \vec{X}_{best} - \left|\vec{X}_{best} - \vec{X}_i(t)\right| \times LevyFlight \tag{19}$$

$$\alpha = \left(\frac{\Gamma(1+\varepsilon) \times \sin(\frac{\pi\varepsilon}{2})}{\Gamma((1+\varepsilon)/2) \times \varepsilon \times 2^{(\frac{\varepsilon-1}{2})}}\right)^{\frac{1}{\varepsilon}} \tag{20}$$

$$LevyFlight = 0.25 \times \frac{\delta \times \alpha}{|\lambda|^{\frac{1}{\varepsilon}}} \tag{21}$$

where $\vec{X}_{best}$ is the best individual in the population; $\Gamma$ is the gamma function; $\varepsilon$ is a constant; $\lambda, \delta$ is a random number between 0 and 1.

Step 3: Get an updated offspring population $N_{off}$, the parent population and the offspring population are combined into a new population $N_n$, stratify the population $N_t$ according to the result of the undominated sort $(F_1, F_2, F_3)$.

Step 4: If $|S_{et}| = N$, all individuals in the previous $F_L$ strata (including the stratum $F_L$) will be the next parent population.

Step 5: If $|S_{et}| > N$, use equation (22)-(24) to normalize the population on $F_L$. Then, linked to the reference points, the k population were selected from the $F_L$ level.

$$ASF(x, \omega) = \max_{j=1,2,\ldots M} \frac{F_i'(x)}{\omega_j} \quad i = 1, 2, \cdots, N \tag{22}$$

$$F_i'(x) = F_i(x) - z_i^{\max} \tag{23}$$

$$\omega_j = \begin{pmatrix} 1 & 10^{-6} & 10^{-6} \\ 10^{-6} & \ddots & 10^{-6} \\ 10^{-6} & 10^{-6} & 1 \end{pmatrix} \tag{24}$$

where $z_i^{\max}$ the extreme point of the $i$th objective; $M$ is the number of objective functions; $F_i'(x)$ is the transformed objective function.

Step 6: If $t > T_{\max}$, terminate the iteration and output the Pareto optimal frontier of the many-objective EV-IES optimization problem; otherwise, return to step 2 to continue the iteration.

**Algorithm 1** The Procedure of MOSCO Algorithm

**Input:** Define the population size $N_p$, the maximum number of iterations $T_{\max}$, Input the initial data of the EV-IES, such as traffic flow, PV output, peak-valley time-of-use electricity pricing, etc.
**Ensure:** The best path of each EV-IES

```
t = 1
Generate parent population N_t
if t ≤ T_max then
  for i = 1 : N_p do
    if rand() ≤ R_1 then % R_1 is a random number between 0 and 1.
      Population update using Equation 17
    elseif rand() > R_1  rand() ≤ R_2%R_2 is a random number between 0 and 1, and R_2 > R_1.
      Population update using Equation 18
    else
      Population update using Equation 19
    end if
  end for
  Get an updated offspring population N_off
  Parents and offspring combine to form a new population N_n = N_t ∪ N_off
  Population N_n was selected as the next parent population N_t by Equation (22)-(24)
  t = t + 1
 end if
```

### B. ETOPSIS

The TOPSIS method is a subjective comprehensive evaluation method that makes full use of the information from the original data, and its results can accurately reflect the gaps between evaluation schemes [35], [36], [37]. The entropy weight method, which calculates the weight of each evaluation index, is also an objective comprehensive evaluation method [38]. Since the TOPSIS method is not sufficient to solve multi-dimensional complex decision problems, this paper applies the ETOPSIS method [39] to determine the optimal operation scheme of the EV-IES from the Pareto solution.

(1) Construction of decision matrix

$$T = \begin{bmatrix} c_{11} & c_{12} & \cdots & c_{1m} \\ c_{21} & c_{22} & \cdots & c_{2m} \\ \vdots & \vdots & \ddots & \vdots \\ c_{n1} & c_{n2} & \cdots & c_{nm} \end{bmatrix} \tag{25}$$

where $m$ denotes the number of evaluation indicators and $n$ denotes the number of evaluation solutions. In the paper, $m$ is the number of objective functions, and $n$ is the number of Pareto solutions.

(2) Normalize the decision matrix according to Equation (26).

$$\begin{cases} X_{ij} = \dfrac{Max_n c_{nm} - c_{nm}}{Max_n c_{nm} - Min_n c_{nm}} \cdots\cdots\cdots (a) \\ X_{ij} = \dfrac{c_{nm} - Min_n c_{nm}}{Max_n c_{nm} - Min_n c_{nm}} \cdots\cdots\cdots (b) \end{cases} \tag{26}$$

where objective function $F1$ is a positive indicator and is normalized using equation (a). Objective functions $F2$ and $F3$ are negative indicators and are normalized using equation (b).

(3) Calculate the entropy value of the $j$th indicator.

$$E_j = -\frac{1}{\ln(n)} \sum_{i=1}^{n} [(X_{ij} \Big/ \sum_{i=1}^{n} X_{ij}) \times \ln(X_{ij} \Big/ \sum_{i=1}^{n} X_{ij})] \quad (27)$$

(4) Calculate the weights of each indicator.

$$\varpi_j = \frac{1 - E_j}{\sum_{j=1}^{m} (1 - E_j)} \quad (28)$$

(5) Construct the weighted decision matrix.

$$A = (\varpi_j a_{ij})_{n \times m} \quad (29)$$

(6) Find the positive and negative ideal solutions of the weighted decision matrix. As in (30), shown at the bottom of the page, where $A_0^+$ is the Positive Ideal Solution (PIS) and $A_0^-$ is the Negative Ideal Solution (NIS). $j^+$ and $j^-$ are positive and negative indicators, respectively.

(7) Calculate the distance between each scheme and the positive and negative ideal points

$$\begin{cases} PISd_i^+ = \sqrt{\sum_{j=1}^{m} (A_0^+ - (\varpi_j c_{ij}))^2} \\ NISd_i^- = \sqrt{\sum_{j=1}^{m} (A_0^- - (\varpi_j c_{ij}))^2} \end{cases} \quad (31)$$

where $PISd_i^+$ and $NISd_i^-$ denote the distance of the $i$th scheme to PIS and NIS, respectively.

(8) Calculate the fit degree of each scheme.

$$\vartheta_i = \frac{NISd_i^-}{PISd_i^+ + PISd_i^-} \quad (32)$$

where a higher $\vartheta_i$ means that this scheme is better. Therefore, the value of $\vartheta_i$ is used to determine the optimal operation scheme.

## IV. OPTIMAL SCHEDULING PLANNING FOR EV-IES

### A. MOSCO ALGORITHM AND MODEL INTEGRATION METHOD

The EV-IES is simulated and modeled in MATLAB, and the traffic flow, PV output, peak-valley time-of-use electricity price, and charging price in each period are input into the EV-IES model as the original data. Then the MOSCO algorithm is used to solve the EV-IES model, and the energy flow of each subsystem is judged. The decision variables are the SOC variation of ESS and electric vehicle battery. Algorithm 2 describes how the decision variables are converted into energy changes and the energy flow of each subsystem.

**Algorithm 2** The Transformation Process of the Decision Variables

**Input:** The population size $N_p$, the maximum number of iterations $T_{\max}$, Input the initial data of the EV-IES. Including traffic flow, PV output, peak-valley time-of-use electricity pricing, the capacity of the ESS, the number of charging post.
**Ensure:** The energy change value of each system
**for** $i = 1 : N_p$ **do**
  $SOC^{\text{ESS}} = SOC_{\min} + (SOC_{\max} - SOC_{\min}) \times [0, 1]$ %$SOC_{\max}$ and $SOC_{\max}$ represent the lower limit and upper limit of the battery capacity of the ESS
  $SOC^{FCSS} = SOC_{\min} + (SOC_{\max} - SOC_{\min}) \times [0, 1]$
**end for**
Using algorithm1 to solve the EV-IES model, the pareto solution set is obtained.
**for** $i = 1 : N_p$ **do**
  **for** $t = 1 : 24$ **do**
    $P_{ESS}(t) = N_B \times B_{cap} \times (SOC_{ESS}(t+1) - SOC_{ESS}(t))$
    $P_{FCSS}(t) = B_{cap} \times (SOC_{FCSS}(t+1) - SOC_{FCSS}(t))$
    **if** $P_{ESS}(t) > 0$ **then** % To determine the ESS is charging or discharging, $P_{ESS}(t) > 0$ indicates charging.
      **if** $P_{PV}(t) \geq P_{ESS}(t) + P_{FCSS}(t)$ **then** % PV output can meet the demand of FSCC and ESS system.
        $P_{ESS}(t) = P_{PV-ESS}(t)$, $P_{FCSS}(t) = P_{PV-FCSS}(t)$% All the energy of ESS and FCSS comes from the PV system.
      **elseif** $P_{PV}(t) \geq P_{ESS}(t)$ $P_{PV}(t) < P_{ESS}(t) + P_{FCSS}(t)$ %PV output can not meet both ESS and FCSS systems, but can meet ESS system.
        $P_{G-FCSS}(t) = P_{FCSS}(t)$-$(P_{PV}(t) - P_{ESS}(t))$, $P_{ESS}(t) = P_{PV-ESS}(t)$ % The PV output preferentially meets the ESS, and the excess energy is transmitted to the FCSS. The rest of the FCSS needs energy from the RPS.
      **else** %PV output does not meet the ESS demand.
        $P_{G-ESS}(t) = P_{ESS}(t) - P_{PV}(t)$, $P_{PV-ESS}(t) = P_{PV}(t)$, $P_{G-FCSS}(t) = P_{FCSS}(t)$, % The energy of ESS comes from PV system and RPS, and the energy of FCSS comes from RPS.
      **end if**
    **else** %$P_{ESS}(t) > 0$ indicates discharging.
      **if** $P_{PV}(t) - P_{ESS}(t) > P_{FCSS}(t)$ % PV output and ESS discharge are greater than FCSS demand.
        $P_{IES-G}(t) = P_{PV}(t) - P_{ESS}(t) - P_{FCSS}(t)$, $P_{FCSS}(t) = P_{FCSS}(t)$ %PV output and ESS discharge are preferentially satisfied with FCSS, and the remaining energy is transmitted to the RPS.
      **else** % PV output and ESS discharge are less than or equal to FCSS demand.
        $P_{G-FCSS}(t) = P_{FCSS}(t) - P_{PV}(t) + P_{ESS}(t)$, $P_{PV-FCSS}(t) = P_{PV}(t)$, $P_{ESS-FCSS}(t) = -P_{ESS}(t)$ %The demand for FCSS comes from PV systems, ESS and RPS.
      **end if**
    **end if**
  **end for**
**end for**

### B. PARAMETER SENSITIVITY ANALYSIS

Aiming at the model of the EV-IES, the different ranges of random numbers in the MOSCO algorithm will affect the experimental results of the model. Therefore, the influence of different ranges of random numbers on the experimental results of the EV-IES is discussed. In sensitivity analysis, the

$$\begin{cases} A_0^+ = \left\{ (\max\limits_{1 \leq i \leq n} (\varpi_j a_{ij}) | j \in j^+, \min\limits_{1 \leq i \leq n} (\varpi_j a_{ij}) | j \in j^-) | i = 1, \cdots, n \right\} \\ A_0^- = \left\{ (\min\limits_{1 \leq i \leq n} (\varpi_j a_{ij}) | j \in j^+, \max\limits_{1 \leq i \leq n} (\varpi_j a_{ij}) | j \in j^-) | i = 1, \cdots, n \right\} \end{cases} \quad (30)$$

population size $N_p = 400$, the maximum number of iterations $T_{\max} = 600$, and each algorithm are run 10 times.

In order to evaluate the solutions obtained by many-objective optimization algorithms, this paper assesses the superiority of the algorithm using five metrics: Spread [40], HV [41], GD [42], IGD [43], and Runtime.

(1) HV: The volume of the region in the target space enclosed by the obtained non-dominated solution set and the reference point, the larger the HV value, the better the comprehensive performance of the algorithm. HV is defined as (33).

$$HV = \delta(\cup_{i=1}^{|S|} v_i) \tag{33}$$

where $\delta$ denotes the Lebesgue measure, which is used to measure the volume; $|S|$ denotes the number of nondominated solution sets, and $v_i$ denotes the hypervolume consisting of the reference point and the $i$th solution in the nondominated solution set.

(2) Spread: It is used to measure the distribution range and propagation degree of the obtained non-dominated solutions. The lower the spread value, the better the distribution and diversity of non-dominant solutions. Spread is defined as (34).

$$\Delta = \frac{d_f + d_l + \sum_{j=1}^{N-1} \left| d_j - \bar{d} \right|}{d_f + d_l + (N-1)\bar{d}} \tag{34}$$

where $d_f$ and $d_l$ denote the Euclidean distance between the extreme solutions and the boundary solutions of the obtained set of non-dominated solutions; $d_j$ is the Euclidean distance between the continuous solutions of the obtained set of non-dominated solutions, and $\bar{d}$ is the average of all $d_j$.

(3) GD: This metric is used to assess the convergence of the obtained solutions. GD is defined as (35).

$$GD = \frac{(\sum_{j=1}^{n} d_j^p)^{1/p}}{n} \tag{35}$$

where $n$ is the total number of Pareto solutions.

(4) IGD: This metric is a comprehensive indicator used to assess the convergence and diversity of obtained solutions. IGD is defined as (36).

$$IGD = \frac{\sum_{j=1}^{n} \left| d_j \right|}{n} \tag{36}$$

(5) Runtime: the length of the operation time indicates the computational complexity of the algorithm, and the longer operation time indicates the higher complexity of the algorithm.

Since the EV-IES model lacks a real Pareto frontier, the specific values of the random numbers $R_1$ and $R_2$ are determined through HV and Spread values. The results are shown in Table 2.

It can be seen from Table 2 that when the average value of HV is optimal and the average value of Spread is suboptimal, $r \leq 0.2$ uses Equation (17) to update the population, $r > 0.2 \&\& r \leq 0.8$ uses Equation (18) to update the population, $r > 0.8$ uses Equation (19) to update the population. When the average value of Spread is optimal, $r \leq 0.6$ uses Equation (17) to update the population, $r > 0.6 \&\& r \leq 0.8$ uses Equation (18) to update the population, $r > 0.8$ uses Equation (19) to update the population. Because the difference between the average values of Spread in these two ranges is not large, the difference between the average values of HV is large. Therefore, when solving the EV-IES model, the random number in the MOSCO algorithm is $r \leq 0.2$ uses Equation (17) to update the population, $r > 0.2 \&\& r \leq 0.8$ uses Equation (18) to update the population, $r > 0.8$ uses Equation (19) to update the population. Therefore, the value of $R_1$ is 0.2, and the value of $R_2$ is 0.8. The flowchart of the MOSCO algorithm for solving the optimal scheduling of the EV-IES is shown in Fig. 3.

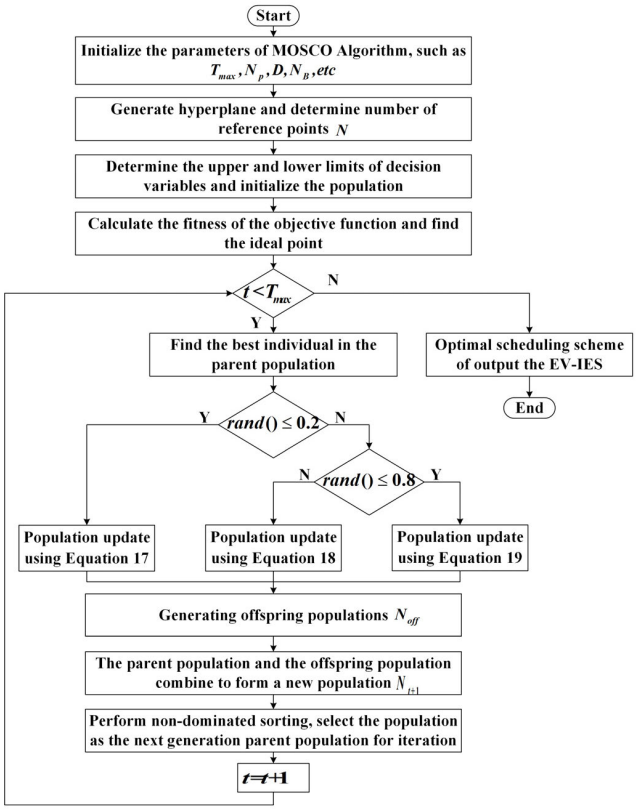


**FIGURE 3.** The flow chart of EV-IES model solved by MOSCO algorithm.

## V. CASE STUDY

Experiments are run in MATLABR2021a with the following computer configurations: an Intel(R) Core (TM) i5-6300HQ CPU running at 2.30 GHz and 8 GB of RAM.

### A. DATA COLLECTION

Sun et al. collected the local information on sunlight intensity and temperature, and calculated the output curve of PV panels by the PV system model [19], as shown in Fig. 4. The peak-to-valley tariff peak-valley time-of-use electricity pricing of

**TABLE 2.** Units for magnetic properties.

| Value ranges | | | HV | Spread |
|---|---|---|---|---|
| Eq. (15) | Eq. (16) | Eq. (17) | | |
| $r \le 0.1$ | $r > 0.1 \& \& r \le 0.9$ | $r > 0.9$ | 1.8480E-1 | 4.6617E-1 |
| $r \le 0.1$ | $r > 0.1 \& \& r \le 0.8$ | $r > 0.8$ | 1.7924E-1 | 4.5645E-1 |
| $r \le 0.1$ | $r > 0.1 \& \& r \le 0.7$ | $r > 0.7$ | 1.8658E-1 | 4.4579E-1 |
| $r \le 0.1$ | $r > 0.1 \& \& r \le 0.5$ | $r > 0.5$ | 1.7460E-1 | 4.7544E-1 |
| $r \le 0.1$ | $r > 0.1 \& \& r \le 0.2$ | $r > 0.2$ | 1.8185E-1 | 4.8220E-1 |
| $r \le 0.2$ | $r > 0.2 \& \& r \le 0.9$ | $r > 0.9$ | 1.8524E-1 | 4.4621E-1 |
| $r \le 0.2$ | $r > 0.2 \& \& r \le 0.8$ | $r > 0.8$ | **2.1800E-1** | 4.4371E-1 |
| $r \le 0.2$ | $r > 0.2 \& \& r \le 0.7$ | $r > 0.7$ | 1.8408E-1 | 4.4995E-1 |
| $r \le 0.2$ | $r > 0.2 \& \& r \le 0.5$ | $r > 0.5$ | 1.8558E-1 | 4.6545E-1 |
| $r \le 0.2$ | $r > 0.2 \& \& r \le 0.3$ | $r > 0.3$ | 1.7789E-1 | 4.8712E-1 |
| $r \le 0.3$ | $r > 0.3 \& \& r \le 0.9$ | $r > 0.9$ | 1.9573E-1 | 4.5015E-1 |
| $r \le 0.3$ | $r > 0.3 \& \& r \le 0.8$ | $r > 0.8$ | 1.9211E-1 | 4.4945E-1 |
| $r \le 0.3$ | $r > 0.3 \& \& r \le 0.7$ | $r > 0.7$ | 1.7600E-1 | 4.7848E-1 |
| $r \le 0.3$ | $r > 0.3 \& \& r \le 0.5$ | $r > 0.5$ | 1.7679E-1 | 4.4699E-1 |
| $r \le 0.3$ | $r > 0.3 \& \& r \le 0.4$ | $r > 0.4$ | 1.8483E-1 | 4.4682E-1 |
| $r \le 0.4$ | $r > 0.4 \& \& r \le 0.9$ | $r > 0.9$ | 1.8732E-1 | 5.0965E-1 |
| $r \le 0.4$ | $r > 0.4 \& \& r \le 0.8$ | $r > 0.8$ | 1.8421E-1 | 4.6323E-1 |
| $r \le 0.4$ | $r > 0.4 \& \& r \le 0.7$ | $r > 0.7$ | 1.8845E-1 | 4.6923E-1 |
| $r \le 0.4$ | $r > 0.4 \& \& r \le 0.6$ | $r > 0.6$ | 1.8523E-1 | 4.6524E-1 |
| $r \le 0.4$ | $r > 0.4 \& \& r \le 0.5$ | $r > 0.5$ | 1.7622E-1 | 4.8145E-1 |
| $r \le 0.5$ | $r > 0.5 \& \& r \le 0.9$ | $r > 0.9$ | 1.8228E-1 | 4.5761E-1 |
| $r \le 0.5$ | $r > 0.5 \& \& r \le 0.8$ | $r > 0.8$ | 1.8653E-1 | 4.4772E-1 |
| $r \le 0.5$ | $r > 0.5 \& \& r \le 0.7$ | $r > 0.7$ | 1.8842E-1 | 4.5522E-1 |
| $r \le 0.5$ | $r > 0.5 \& \& r \le 0.6$ | $r > 0.6$ | 1.9624E-1 | 4.5317E-1 |
| $r \le 0.6$ | $r > 0.6 \& \& r \le 0.9$ | $r > 0.9$ | 1.8295E-1 | 4.7532E-1 |
| $r \le 0.6$ | $r > 0.6 \& \& r \le 0.8$ | $r > 0.8$ | 1.8186E-1 | **4.4244E-1** |
| $r \le 0.6$ | $r > 0.6 \& \& r \le 0.7$ | $r > 0.7$ | 1.8653E-1 | 4.7761E-1 |
| $r \le 0.7$ | $r > 0.7 \& \& r \le 0.9$ | $r > 0.9$ | 1.8062E-1 | 4.5035E-1 |
| $r \le 0.7$ | $r > 0.7 \& \& r \le 0.8$ | $r > 0.8$ | 1.7830E-1 | 4.4883E-1 |
| $r \le 0.8$ | $r > 0.8 \& \& r \le 0.9$ | $r > 0.9$ | 1.6994E-1 | 4.7383E-1 |

the Wuhan RPS is shown in Fig. 5. During periods of high demand in the RPS, it corresponds to the peak electricity price for the EV-IES. Conversely, during periods of low demand, it corresponds to the off-peak electricity price for the EV-IES.

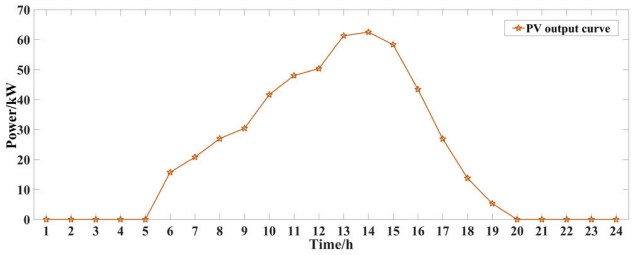


**FIGURE 4.** Photovoltaic output curve.

Liu et al. [44] modeled the charging time from EVs to fast charging stations; Liu et al. [45] fitted the final travel end curve of EV owners through the survey data of the whole family travel; the model of the two can be described as Equation (37), and is normally distributed. It shows that the traffic flow of the EV-IES conforms to the normal distribution. The number of EV charging in each period of

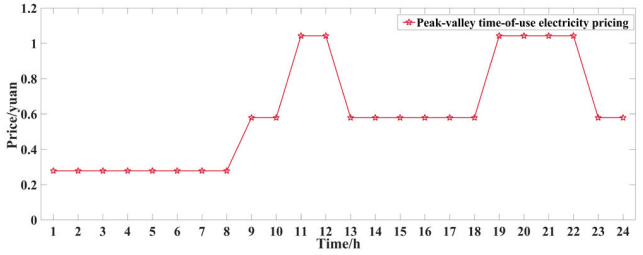


**FIGURE 5.** Peak-valley time-of-use electricity pricing.

multiple local fast charging stations is counted, the proportion is reduced, and the curve that basically conforms to the normal distribution is fitted. The specific data of traffic flow are shown in Fig. 6, which is used as the traffic flow of the EV-IES in this paper.

In the EV-IES model, the priority is to meet the charging demand of EV users in each time period. By determining the decision variable, which is the product of the EV users of battery SOC variation and the traffic flow, we can obtain the charging load of the FCSS for each time period.

$$N(t) = \begin{cases} \dfrac{1}{\delta_N \sqrt{2\pi}} \exp\left[-\dfrac{(t-\mu_N)^2}{2\delta_N^2}\right] \\ (\mu_N - 12) < t \le 24 \\ \dfrac{1}{\delta_N \sqrt{2\pi}} \exp\left[-\dfrac{(t+24-\mu_N)^2}{2\delta_N^2}\right] \\ 0 < t \le (\mu_N - 12) \end{cases} \tag{37}$$

where $\mu_N = 17.6$, $\sigma_N = 3.4$; t is the moment of charging.

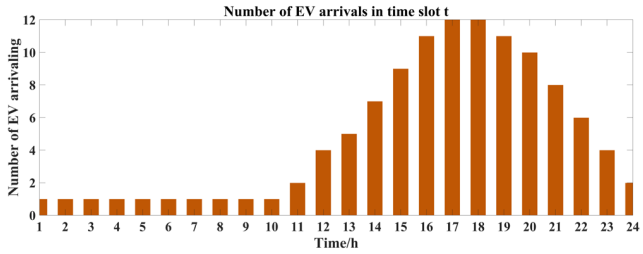


**FIGURE 6.** Number of electric vehicle arrivals by time period.

### B. CASE STUDY SETTING

(1) Case 1.

In this case, there is no PV and BESS in the EV-IES model, directly connected to the RPS. It belongs to a typical traditional charging station model. Since the FCSS does not involve feeding power back to the RPS, objective function $F2$ is positively correlated with $F3$. Therefore, in Case 1, only objective functions $F1$ and $F3$ are optimized. This case needs to satisfy the constraints (8)-(10) and (13).

(2) Case 2.

In this case, there is no BESS in the EV-IES model. The power required by the model is composed of two parts. One

part comes from the PV system, and the other part comes from the RPS. Because Case 2 has the same problem as Case 1, it optimizes only objective functions $F1$ and $F3$. This case needs to satisfy the constraints (8)-(10) and (13).

(3) Case 3.

In Case 3, there is no PV in the EV-IES model. In Case 3, there is no PV system in the EV-IES model. The primary distinction from the EV-IES model is the absence of the PV generation component. Case 3 is optimized for objective functions $F1$, $F2$, and $F3$ because it has an ESS involving power feedback from the storage system to the RPS. This case needs to satisfy the constraints (7)-(16).

**TABLE 3. Components of each case.**

| | PV | ESS |
|---|---|---|
| *Case1* | No | No |
| *Case2* | Yes | No |
| *Case3* | No | Yes |
| *Case4* | Yes | Yes |

Table 3 shows the difference between cases and the EV-IES model designed in this paper. Case 1 represents the traditional charging station model. Case4 is the model designed in this paper.

### C. RESULTS DISCUSSION

#### 1) ALGORITHM COMPARISON BY BENCHMARK FUNCTIONS

NSGA-III [46], an Adaptive-reference-point-based Nondominated Sorting Genetic Algorithm (ANSGA-III) [47], a Grouped and Linked Mutation Operator (GLMO) algorithm [48], a Theta Dominance based Evolutionary Algorithm (t-DEA) [49], and NSGA-II [50] are compared with the MOSCO algorithm to verify the effectiveness. In these six algorithms, the population size $N_p = 400$, and each algorithm are run 10 times in this paper.

Because the DTLZ series of functions have real Pareto fronts, we use IGD and GD to evaluate the simulation results of these six algorithms. Detailed data on the IGD and GD obtained by the six algorithms are provided in Tables 4 and 5.

Based on the data in Tables 4 and 5, it can be observed that the MOSCO algorithm outperforms the other five algorithms in terms of IGD and GD values in most cases, including best, average, and worst values. By analyzing the GD and IGD values, it can be demonstrated that the algorithm exhibits excellent convergence and solution set diversity. This indicates that the MOSCO algorithm excels in effectively addressing many-objective problems. The reason why the MOSCO algorithm excels is because it cleverly incorporates both global search and Levy strategies to enhance its performance. The global search strategy helps the algorithm rapidly discover optimal solution sets, thereby improving convergence speed. Meanwhile, the Levy strategy effectively prevents the algorithm from getting trapped in local optima. As a result, the MOSCO algorithm not only demonstrates remarkable convergence but also possesses the capability to avoid falling into local optima. It shows that the MOSCO algorithm has good solving ability.

#### 2) ALGORITHM COMPARISON BY THE EV-IES MODEL

NSGA-III, ANSGA-III, GLMO, t-DEA, and NSGA-II are compared with the MOSCO algorithm to verify the effectiveness. Fig. 7 shows the results of the six algorithms for solving the optimal scheduling model of the EV-IES. In these six algorithms, the population size $N_p = 400$, the maximum number of iterations $T_{\max} = 600$, and each algorithm are run 10 times in this paper.

Since the designed EV-IES model does not have a real Pareto front, GD and IGD cannot be used to evaluate the optimized scheduling results of the EV-IES. Therefore, three indicators, HV, Runtime, and Spread, are used to evaluate the optimal scheduling results of the six algorithms.

The comparison of Spread, HV, and Runtime obtained by NSGA-III, ANSGA-III, GLMO, t-DEA, NSGA-II, and the MOSCO algorithm is shown in Tables 6, 7, and 8, respectively.

As can be seen from the spread evaluation index in Table 6, no matter the ''Best'', ''Mean'' and ''Worst'' Spreads, the MOSCO algorithm solves the non-dominated solution set with a smaller Spread value than the other five algorithms. It shows that the distribution of the non-dominated solution set solved by the MOSCO algorithm is more uniform. As shown in the HV evaluation index in Table 7, the MOSCO algorithm has the best ''Best'' and ''Mean'' HV evaluation indices among the six algorithms, with the ''Worst'' HV value index being second only to the NSGA-II algorithm. As shown in the runtime evaluation index in Table 8, The runtime of the MOSCO algorithm is second only to NSGA-II, indicating that the MOSCO algorithm exhibits excellent convergence. It proves that the MOSCO algorithm has good comprehensive performance.

Based on the HV, Spread, and running time results of the MOSCO algorithm and the other five algorithms for solving the Pareto solution set of the EV-IES model, it shows that the Pareto solution set solved by the MOSCO algorithm is superior to the other five algorithms.

#### 3) ANALYSIS OF MODEL RESULTS

(1) Case 1

In case 1, the decision variable is the SOC change of the EV battery of FCSS users. The objective functions of the optimal operation scheme in case 1 are as follows: $F1 = 1981.96yuan$ and $F3 = 3615.87kg$. The hourly load profile of the FCSS is depicted in Fig. 8. When compared to the optimal operating scheme in case 4, the daily revenue in case 1 has decreased by 21.86%, while pollutant emissions have increased by 25.30%.

(2) Case 2

In case 2, the output curve of the PV system is shown in Fig. 4, and the decision variables are the same as those in case 1. The objective functions of the optimal operation scheme in case 2 are as follows: $F1 = 2306.26yuan$ and

**TABLE 4.** GD obtained by different algorithms.

| Problem | M | $T_{max}$ | NSGA-II | NSGA-III | ANSGA-III | t-DEA | GLMO | MOSCO |
|---|---|---|---|---|---|---|---|---|
| DTLZ1 | 3 | 600 | **9.1992E-05** | 9.4614E-05 | 9.4250E-05 | 9.5225E-05 | 1.9656E-04 | 9.3489E-05 |
| | | | 1.1611E-04 | 9.5280E-05 | 2.8721E-02 | 9.5690E-05 | 2.3099E-04 | **9.4717E-05** |
| | | | 2.7169E-04 | 9.5852E-05 | 2.6215E-01 | 9.6257E-05 | 2.8898E-04 | **9.5266E-05** |
| | 5 | 800 | 1.6700E-03 | 8.8670E-04 | 8.5830E-04 | 8.8523E-04 | 9.6786E-04 | **8.4357E-04** |
| | | | 3.9044E-03 | 8.8759E-04 | 8.9987E-03 | 8.8634E-04 | 1.0149E-03 | **8.8445E-04** |
| | | | 1.9558E-02 | 8.9167E-04 | 8.1978E-02 | **8.8723E-04** | 1.0603E-03 | 9.0921E-04 |
| | 10 | 1000 | 1.5845E+01 | 8.3742E-04 | 2.1507E-03 | 8.4684E-04 | 1.2659E-03 | **6.2150E-04** |
| | | | 1.7948E+01 | 9.4545E-04 | 2.2090E-01 | 8.6031E-04 | 9.9016E-02 | **7.6502E-04** |
| | | | 1.1561E+01 | 1.6886E-03 | 1.1464E+00 | 9.0873E-04 | 6.8966E-01 | **9.0400E-04** |
| DTLZ2 | 3 | 600 | 4.1243E-04 | 2.5450E-04 | 2.5492E-04 | 2.5568E-04 | 2.6392E-04 | **2.5318E-04** |
| | | | 4.3847E-04 | 2.5592E-04 | 2.6378E-04 | 2.5623E-04 | 2.6752E-04 | **2.5797E-04** |
| | | | 4.8432E-04 | **2.5726E-04** | 2.7179E-04 | 2.5739E-04 | 2.7662E-04 | 2.6683E-04 |
| | 5 | 800 | 4.8239E-03 | 2.8791E-03 | 2.8510E-03 | 2.8767E-03 | 2.8734E-03 | **2.8092E-03** |
| | | | 5.4930E-03 | 2.8813E-03 | 2.8697E-03 | 2.8784E-03 | 2.8841E-03 | **2.8572E-03** |
| | | | 6.7004E-03 | 2.8857E-03 | 2.8886E-03 | 2.8800E-03 | 2.8907E-03 | **2.8786E-03** |
| | 10 | 1000 | 1.2044E-01 | 3.7569E-03 | 4.8829E-03 | 3.7421E-03 | 4.0511E-03 | **3.4109E-03** |
| | | | 1.2122E-01 | 3.7840E-03 | 7.1598E-03 | 3.7633E-03 | 4.9742E-03 | **3.4737E-03** |
| | | | 1.2172E-01 | 3.8412E-03 | 8.3953E-03 | **3.7932E-03** | 1.1819E-02 | 3.8269E-03 |
| DTLZ3 | 3 | 600 | 2.6468E-04 | 2.5385E-04 | 2.5350E-04 | 2.5430E-04 | 1.7896E-02 | **2.3516E-04** |
| | | | 2.9676E-04 | 2.5840E-04 | 6.6407E-02 | 2.5721E-04 | 2.3849E-02 | **2.5362E-04** |
| | | | 4.0850E-04 | 2.7853E-04 | 5.9163E-01 | 2.6066E-04 | 3.1125E-02 | **2.5819E-04** |
| | 5 | 800 | 3.5132E-01 | 2.8654E-03 | **2.6288E-03** | 2.8616E-03 | 4.5045E-03 | 2.7349E-03 |
| | | | 7.4100E-01 | 2.8713E-03 | 6.3925E-02 | 2.8689E-03 | 2.1435E-01 | **2.7857E-03** |
| | | | 1.1938E+00 | 2.8752E-03 | 6.1399E-01 | 2.8743E-03 | 1.0178E+00 | **2.8171E-03** |
| | 10 | 1000 | 1.0148E+02 | 3.7960E-03 | 2.1302E+00 | 3.7997E-03 | 7.5588E-03 | **3.7039E-03** |
| | | | 1.0271E+02 | 9.2315E-01 | 2.7585E+00 | 2.7363E-01 | 7.9883E+00 | **2.7361E-01** |
| | | | 1.0386E+02 | 3.7379E+00 | 4.1190E+00 | 2.7018E+00 | 3.8861E+01 | **2.7009E+00** |
| DTLZ4 | 3 | 600 | 4.0650E-04 | 2.5382E-04 | 2.5788E-04 | 2.5472E-04 | 2.6622E-04 | **2.5187E-04** |
| | | | 4.4394E-04 | 2.5711E-04 | 2.6490E-04 | 2.5685E-04 | 2.7603E-04 | **2.5587E-04** |
| | | | 4.7187E-04 | 2.6756E-04 | 2.7366E-04 | 2.6191E-04 | 3.0154E-04 | **2.5972E-04** |
| | 5 | 800 | 4.7219E-03 | 2.8741E-03 | 2.8267E-03 | 2.8690E-03 | 2.8691E-03 | **2.8256E-03** |
| | | | 5.3635E-03 | 2.8780E-03 | 2.8605E-03 | 2.8729E-03 | 2.8960E-03 | **2.8471E-03** |
| | | | 6.1298E-03 | 2.8819E-03 | 2.8848E-03 | 2.8775E-03 | 2.9165E-03 | **2.8723E-03** |
| | 10 | 1000 | 1.1827E-01 | 3.6921E-03 | 3.7121E-03 | 3.6938E-03 | 3.9413E-03 | **3.1833E-03** |
| | | | 1.1985E-01 | 3.7557E-03 | 4.7226E-03 | 3.7334E-03 | 4.0754E-03 | **3.4451E-03** |
| | | | 1.2067E-01 | 3.8228E-03 | 8.6527E-03 | 3.7660E-03 | 4.2607E-03 | **3.7350E-03** |
| DTLZ5 | 3 | 600 | 2.2754E-05 | 2.9520E-05 | 2.3602E-05 | 1.2826E-05 | 8.1745E-05 | **1.1690E-05** |
| | | | 2.7335E-05 | 4.2294E-05 | 4.0182E-05 | 3.4760E-05 | 9.8272E-05 | **1.7014E-05** |
| | | | 3.8847E-05 | 6.0295E-05 | 5.9015E-05 | 8.6923E-05 | 1.2618E-04 | **2.6875E-05** |
| | 5 | 800 | 8.0731E-02 | 7.2411E-02 | 7.9355E-02 | **6.8601E-02** | 7.5364E-02 | 7.2052E-02 |
| | | | 8.3078E-02 | 7.9230E-02 | 8.3803E-02 | 7.8487E-02 | 8.0219E-02 | **7.6148E-02** |
| | | | 8.4549E-02 | 8.5390E-02 | 9.0103E-02 | 8.4515E-02 | 8.4359E-02 | **7.8416E-02** |
| | 10 | 1000 | 1.1962E-01 | 8.5654E-02 | 7.4184E-02 | **6.3427E-02** | 8.6385E-02 | 8.2311E-02 |
| | | | 1.2193E-01 | 8.8735E-02 | 8.6982E-02 | 8.9546E-02 | 9.4294E-02 | **8.4595E-02** |
| | | | 1.2431E-01 | 9.3230E-02 | 9.9871E-02 | 1.0858E-01 | 9.8338E-02 | **8.8705E-02** |
| DTLZ6 | 3 | 600 | 2.3350E-06 | 2.2936E-06 | **2.1766E-06** | 2.4088E-06 | 2.2090E-06 | 2.3192E-06 |
| | | | 2.4058E-06 | 2.3973E-06 | **2.3500E-06** | 2.5969E-06 | 4.0393E-04 | 2.3526E-06 |
| | | | 2.5099E-06 | 2.5974E-06 | 2.5153E-06 | 2.7283E-06 | 4.0181E-03 | **2.3991E-06** |
| | 5 | 800 | 2.9129E-01 | 1.5654E-01 | 1.5144E-01 | **1.2672E-01** | 1.8482E-01 | 1.4113E-01 |
| | | | 3.0136E-01 | 1.8605E-01 | 1.7743E-01 | 1.5178E-01 | 2.1767E-01 | **1.4901E-01** |
| | | | 3.0742E-01 | 2.1208E-01 | 2.0189E-01 | 2.5324E-01 | 2.5039E-01 | **1.5944E-01** |
| | 10 | 1000 | 4.9994E-01 | 2.3466E-01 | 3.2167E-01 | 1.0823E-01 | 2.5985E-01 | **1.0169E-01** |
| | | | 5.0322E-01 | 2.8372E-01 | 3.6198E-01 | 1.2061E-01 | 3.3043E-01 | **1.1476E-01** |
| | | | 5.0689E-01 | 3.3742E-01 | 4.0334E-01 | 1.4016E-01 | 4.1119E-01 | **1.3606E-01** |
| DTLZ7 | 3 | 600 | 6.9671E-04 | 6.0400E-04 | 5.4398E-04 | 4.2241E-04 | 5.4313E-04 | **3.1718E-04** |
| | | | 7.7989E-04 | 6.7634E-04 | 6.0495E-04 | 5.1835E-04 | 6.2896E-04 | **3.7450E-04** |
| | | | 8.5247E-04 | 7.4000E-04 | 6.6378E-04 | 6.4078E-04 | 7.3344E-04 | **4.5144E-04** |
| | 5 | 800 | 9.7592E-03 | 5.8658E-03 | 5.8258E-03 | **4.5690E-03** | 6.0120E-03 | 5.2996E-03 |
| | | | 1.0390E-02 | 6.2170E-03 | 6.1106E-03 | 5.4619E-03 | 6.3555E-03 | **5.3523E-03** |
| | | | 1.0925E-02 | 6.6249E-03 | 6.3414E-03 | 6.3737E-03 | 6.8372E-03 | **5.4523E-03** |
| | 10 | 1000 | 1.6240E+00 | 2.2019E-02 | 2.1494E-02 | 2.0246E-02 | 2.2576E-02 | **2.0147E-02** |
| | | | 1.7301E+00 | 2.2841E-02 | 2.2493E-02 | 2.5350E-02 | 2.4489E-02 | **2.2330E-02** |
| | | | 1.8826E+00 | 2.3997E-02 | 2.4426E-02 | 2.9804E-02 | 2.8150E-02 | **2.3656E-02** |

**TABLE 5.** IGD obtained by different algorithms.

| Problem | M | $T_{max}$ | NSGA-II | NSGA-III | ANSGA-III | t-DEA | GLMO | MOSCO |
|---|---|---|---|---|---|---|---|---|
| DTLZ1 | 3 | 600 | 1.2929E-02 | 9.4875E-03 | 9.6390E-03 | 9.4866E-03 | 1.0546E-02 | **9.4534E-03** |
| | | | 1.3374E-02 | 9.4883E-03 | 1.2797E-02 | 9.4881E-03 | 1.0751E-02 | **9.4775E-03** |
| | | | 1.3902E-02 | 9.4906E-03 | 1.8716E-02 | **9.4890E-03** | 1.1005E-02 | 9.4922E-03 |
| | 5 | 800 | 6.1886E-02 | 4.5254E-02 | 4.5199E-02 | 4.5244E-02 | 4.5812E-02 | **4.2375E-02** |
| | | | 8.8862E-02 | 4.5259E-02 | 4.6690E-02 | 4.5251E-02 | 4.6198E-02 | **4.3446E-02** |
| | | | 3.0061E-01 | 4.5281E-02 | 5.7994E-02 | 4.5254E-02 | 4.6795E-02 | **4.4294E-02** |
| | 10 | 1000 | 2.2232E+00 | 1.0867E-01 | 1.1075E-01 | 1.0763E-01 | 1.0647E-01 | **1.0482E-01** |
| | | | 8.7979E+00 | 1.0899E-01 | 1.3623E-01 | 1.0812E-01 | 1.2047E-01 | **1.0590E-01** |
| | | | 1.5605E+01 | 1.0933E-01 | 2.2523E-01 | 1.0873E-01 | 1.7611E-01 | **1.0765E-01** |
| DTLZ2 | 3 | 600 | 3.3596E-02 | 2.5211E-02 | 2.5337E-02 | 2.5210E-02 | 2.5227E-02 | **2.5052E-02** |
| | | | 3.4308E-02 | 2.5215E-02 | 2.5619E-02 | 2.5212E-02 | 2.5232E-02 | **2.5197E-02** |
| | | | 3.5106E-02 | 2.5226E-02 | 2.5848E-02 | **2.5214E-02** | 2.5241E-02 | 2.5239E-02 |
| | 5 | 800 | 1.6747E-01 | 1.4179E-01 | 1.4178E-01 | 1.4178E-01 | 1.4187E-01 | **1.3875E-01** |
| | | | 1.7443E-01 | 1.4180E-01 | 1.4194E-01 | 1.4179E-01 | 1.4193E-01 | **1.4056E-01** |
| | | | 1.7933E-01 | 1.4184E-01 | 1.4221E-01 | 1.4179E-01 | 1.4201E-01 | **1.4133E-01** |
| | 10 | 1000 | 1.6995E+00 | 4.2053E-01 | 4.2188E-01 | 4.2043E-01 | 4.2214E-01 | **4.0203E-01** |
| | | | 2.3269E+00 | 4.2128E-01 | 4.4350E-01 | 4.2103E-01 | 4.4567E-01 | **4.1107E-01** |
| | | | 2.4336E+00 | 4.2189E-01 | 5.0230E-01 | 4.2134E-01 | 6.5129E-01 | **4.1708E-01** |
| DTLZ3 | 3 | 600 | 3.3499E-02 | 2.5216E-02 | 2.6662E-02 | 2.5220E-02 | 1.9110E-01 | **2.5112E-02** |
| | | | 3.4278E-02 | 2.5242E-02 | 3.4305E-02 | 2.5228E-02 | 2.4914E-01 | **2.5139E-02** |
| | | | 3.5355E-02 | 2.5408E-02 | 7.5540E-02 | 2.5251E-02 | 3.0251E-01 | **2.5163E-02** |
| | 5 | 800 | 1.7626E-01 | 1.4177E-01 | 1.4302E-01 | 1.4175E-01 | 1.5018E-01 | **1.4113E-01** |
| | | | 1.8550E-01 | 1.4182E-01 | 1.4785E-01 | 1.4176E-01 | 1.5311E-01 | **1.4138E-01** |
| | | | 1.9748E-01 | 1.4193E-01 | 1.6012E-01 | 1.4178E-01 | 1.5724E-01 | **1.4166E-01** |
| | 10 | 1000 | 1.0314E+03 | 4.1884E-01 | 5.2031E-01 | 4.1885E-01 | **4.1438E-01** | 4.1885E-01 |
| | | | 1.3838E+03 | 4.8392E-01 | 5.7323E-01 | 4.3612E-01 | 1.2323E+01 | **4.3842E-01** |
| | | | 1.6998E+03 | 6.3291E-01 | 6.5949E-01 | 5.8400E-01 | 1.1739E+02 | **5.8400E-01** |
| DTLZ4 | 3 | 600 | 3.3185E-02 | 2.5212E-02 | 2.5378E-02 | 2.5211E-02 | 2.5308E-02 | **2.5023E-02** |
| | | | 3.4239E-02 | 2.5228E-02 | 2.5633E-02 | 2.5234E-02 | 2.5385E-02 | **2.5210E-02** |
| | | | 3.5488E-02 | **2.5259E-02** | 2.6395E-02 | 2.5313E-02 | 2.5562E-02 | 2.5342E-02 |
| | 5 | 800 | 1.6839E-01 | 1.4178E-01 | 1.4178E-01 | 1.4177E-01 | 1.4208E-01 | **1.4041E-01** |
| | | | 1.7113E-01 | 1.4641E-01 | 1.4211E-01 | 1.4177E-01 | 1.4219E-01 | **1.4125E-01** |
| | | | 1.7451E-01 | 1.8789E-01 | 1.4258E-01 | **1.4178E-01** | 1.4232E-01 | 1.4195E-01 |
| | 10 | 1000 | 1.5088E+00 | 4.1980E-01 | 4.1948E-01 | 4.1949E-01 | 4.2055E-01 | **4.1251E-01** |
| | | | 1.9759E+00 | 4.2038E-01 | 4.2805E-01 | 4.2018E-01 | 4.2126E-01 | **4.1747E-01** |
| | | | 2.3815E+00 | **4.2100E-01** | 4.9958E-01 | 4.2134E-01 | 4.2281E-01 | 4.2215E-01 |
| DTLZ5 | 3 | 600 | 1.3657E-03 | 2.6490E-03 | 2.2846E-03 | 1.1995E-02 | 2.3609E-03 | **1.1597E-03** |
| | | | 1.3998E-03 | 3.0071E-03 | 2.4229E-03 | 1.3680E-02 | 2.8684E-03 | **1.2855E-03** |
| | | | **1.4626E-03** | 3.4869E-03 | 2.5703E-03 | 1.5265E-02 | 3.3073E-03 | 1.5264E-03 |
| | 5 | 800 | **1.9041E-02** | 4.3078E-02 | 3.7388E-02 | 6.0266E-02 | 4.8865E-02 | 2.1488E-02 |
| | | | **2.9196E-02** | 6.2743E-02 | 6.6729E-02 | 9.6996E-02 | 7.0787E-02 | 3.8825E-02 |
| | | | 6.5436E-02 | 9.9493E-02 | 1.1135E-01 | 1.5358E-01 | 1.0670E-01 | **5.1072E-02** |
| | 10 | 1000 | 4.6170E-02 | 1.8488E-01 | 1.5186E-01 | 1.2398E-01 | 1.8549E-01 | **1.0465E-02** |
| | | | 8.7739E-02 | 3.7972E-01 | 3.8313E-01 | 1.8714E-01 | 3.4804E-01 | **1.7517E-02** |
| | | | 1.3264E-01 | 5.3197E-01 | 5.1225E-01 | 2.7686E-01 | 4.8307E-01 | **2.7186E-02** |
| DTLZ6 | 3 | 600 | 1.3800E-03 | 4.4303E-03 | 2.7633E-03 | 1.3085E-02 | 3.3000E-03 | **1.2372E-03** |
| | | | 1.4298E-03 | 4.7373E-03 | 3.0677E-03 | 1.6208E-02 | 4.0602E-03 | **1.3202E-03** |
| | | | 1.4678E-03 | 5.2980E-03 | 3.3518E-03 | 1.7519E-02 | 5.1017E-03 | **1.3973E-03** |
| | 5 | 800 | 4.9162E-02 | 8.7323E-02 | 8.2296E-02 | 1.3089E-01 | 7.0775E-02 | **2.7355E-02** |
| | | | 8.9336E-02 | 1.3476E-01 | 1.7371E-01 | 1.6749E-01 | 1.2811E-01 | **4.9173E-02** |
| | | | 2.2498E-01 | 2.0490E-01 | 2.9573E-01 | 2.0334E-01 | 2.7795E-01 | **6.6158E-02** |
| | 10 | 1000 | 4.0720E+00 | 1.8998E-01 | 3.2346E-01 | 2.2509E-01 | 2.1590E-01 | **6.0567E-02** |
| | | | 5.0739E+00 | 5.9886E-01 | 6.1644E-01 | 2.9974E-01 | 6.4166E-01 | **8.7932E-02** |
| | | | 6.2313E+00 | 1.1020E+00 | 1.1912E+00 | 3.5549E-01 | 1.1997E+00 | **1.4870E-01** |
| DTLZ7 | 3 | 600 | 3.3274E-02 | 3.3001E-02 | 3.2433E-02 | 3.9032E-02 | 3.2073E-02 | **3.1523E-02** |
| | | | 3.4828E-02 | 3.3782E-02 | 3.3050E-02 | 4.0614E-02 | 3.3014E-02 | **3.2133E-02** |
| | | | 3.6317E-02 | 3.4525E-02 | 3.3714E-02 | 4.2640E-02 | 3.3946E-02 | **3.2692E-02** |
| | 5 | 800 | 2.4277E-01 | 2.4352E-01 | 2.4872E-01 | 2.5222E-01 | 2.4131E-01 | **2.4099E-01** |
| | | | 2.5095E-01 | 2.5032E-01 | 2.5533E-01 | 2.5904E-01 | 2.5079E-01 | **2.4541E-01** |
| | | | 2.5944E-01 | 2.5560E-01 | 2.6272E-01 | 2.7619E-01 | 2.6148E-01 | **2.5489E-01** |
| | 10 | 1000 | 1.5950E+00 | **8.4955E-01** | 8.6495E-01 | 8.8231E-01 | 9.1405E-01 | 8.5444E-01 |
| | | | 1.6521E+00 | 8.9850E-01 | 9.5517E-01 | 9.4299E-01 | 9.9559E-01 | **8.6499E-01** |
| | | | 1.7436E+00 | 9.5828E-01 | 1.1180E+00 | 1.2136E+00 | 1.1849E+00 | **8.8924E-01** |

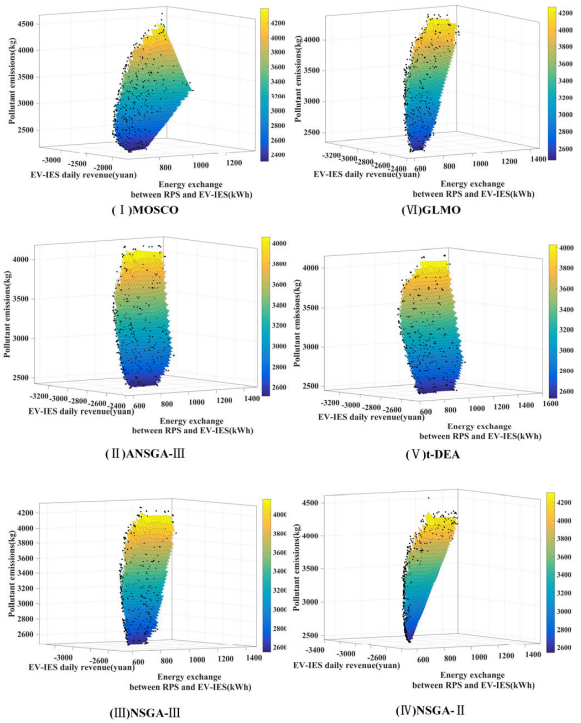


**FIGURE 7.** The Pareto solution sets obtained by solving the EV-IES using six different algorithms. (I)Results of MOSCO; (II) Results of ANSGA-III; (III) Results of NSGA-III; (IV) Results of GLMO; (V) Results of t-DEA; (VI) Results of NSGA-II.

**TABLE 6.** Comparisons of the spread indicator.

| Algorithm | Spread | | |
|---|---|---|---|
| | Best | Mean | Worst |
| *ANSGA-Ⅲ* | 4.8867E-1 | 5.3650E-1 | 5.8834E-1 |
| *NSGA-Ⅲ* | 5.0348E-1 | 5.5448E-1 | 5.9170E-1 |
| *GLMO* | 4.0816E-1 | 4.5134E-1 | 5.3931E-1 |
| *t-DEA* | 6.2669E-1 | 7.0639E-1 | 7.8817E-1 |
| *NSGA-Ⅱ* | 4.9810E-1 | 5.3737E-1 | 5.6641E-1 |
| *MOSCO* | **4.0296E-1** | **4.4371E-1** | **4.8197E-1** |

**TABLE 7.** Comparisons of the HV indicator.

| Algorithm | HV | | |
|---|---|---|---|
| | Best | Mean | Worst |
| *ANSGA-Ⅲ* | 1.7937E-1 | 1,6758E-1 | 1.5137E-1 |
| *NSGA-Ⅲ* | 1.7975E-1 | 1.6838E-1 | 1.5456E-1 |
| *GLMO* | 1.8205E-1 | 1.7010E-1 | 1.5839E-1 |
| *t-DEA* | 1.6450E-1 | 1.5348E-1 | 1.4235E-1 |
| *NSGA-Ⅱ* | 2.0460E-1 | 1.9443E-1 | **1.8623E-1** |
| *MOSCO* | **3.3993E-1** | **2.1800E-1** | 1.7758E-1 |

$F3 = 3104.53kg$. When compared to the optimal operating scheme in case 4, the daily revenue in case 2 has decreased by 10.00%, while pollutant emissions have increased by 7.58%. The hourly load profiles of the RPS and the FCSS are illustrated in Fig. 9.

(3) case 3

In case 3, the decision variables encompass the SOC change of the ESS and the EV battery of FCSS users. The Pareto solutions are illustrated in Fig. 11. The objective functions of the optimal operation scheme in case 3 are as

**TABLE 8.** Comparisons of the runtime indicator.

| Algorithm | Runtime (seconds) | | |
|---|---|---|---|
| | Best | Mean | Worst |
| *ANSGA-Ⅲ* | 40.994 | 57.119 | 67.136 |
| *NSGA-Ⅲ* | 21.072 | 30.078 | 34.096 |
| *GLMO* | 30.745 | 45.134 | 49.461 |
| *t-DEA* | 22.042 | 43.364 | 41.318 |
| *NSGA-Ⅱ* | 10.553 | 13.3372 | 14.876 |
| *MOSCO* | 19.014 | 26.409 | 33.993 |

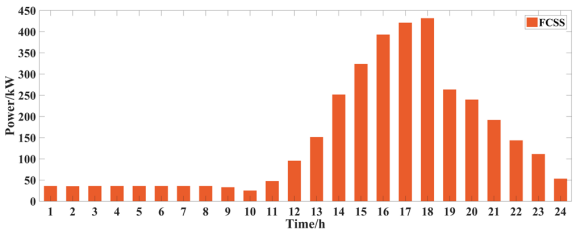


**FIGURE 8.** The power load of fast charging service station.

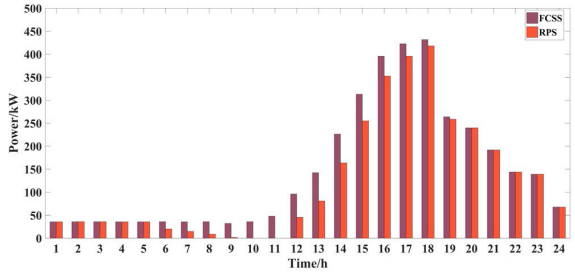


**FIGURE 9.** The power load of FCSS and regional power systems.

follows: $F1 = 1981.96yuan$, $F2 = 833.80kWh$, and $F3 = 3615.87kg$. When compared to the optimal operating scheme in case 4, the daily revenue in case 3 has decreased by 17.41%, the exchanged energy between the RPS and the EV-IES has increased by 5.69%, and pollutant emissions have increased by 8.69%. The hourly input/output values for ESS, RPS, and FCSS are depicted in Fig. 10.

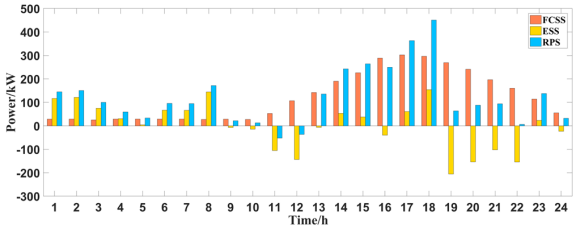


**FIGURE 10.** The output power of FCSS, ESS and regional power systems.

(3) case 4

This study designs a set of EV-IES models to quantitatively analyze the hourly subsystem and RPS energy flows. Based on the collected data for the experimental simulation, the optimization model is solved by the MOSCO algorithm, and the Pareto solution is obtained, as shown in Fig. 12.

Since only one safe and stable operation scheme is required for the EV-IES. Therefore, the ETOPSIS method is applied to determine the optimal operation scheme of the EV-IES from the Pareto solutions. In the optimal operation scheme, the daily revenue of the EV-IES is 2536.33 yuan, the exchanged

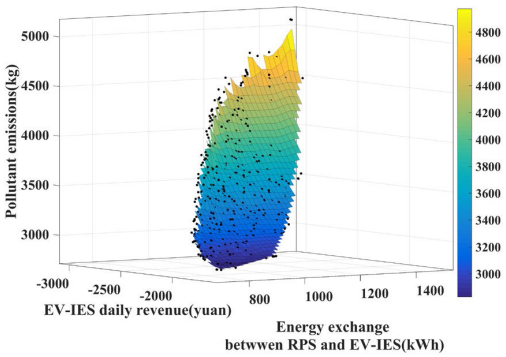


**FIGURE 11.** MOSCO algorithm is used to solve the pareto solution set of case3.

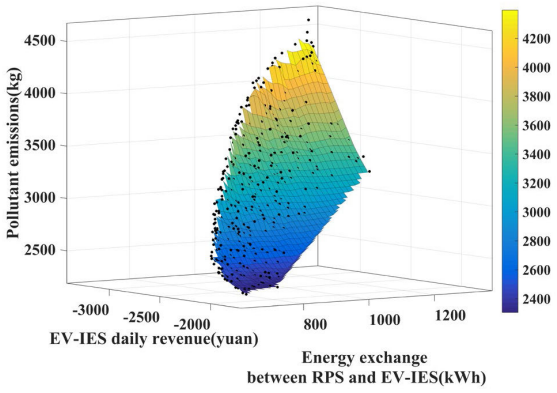


**FIGURE 12.** MOSCO algorithm is used to solve the pareto solution set of case4.

energy between the RPS and the EV-IES is 788.91 kWh, and the pollutant emission is 2885.87 kg. The hourly input/output values of the ESS, the RPS, and the FCSS are shown in Fig. 13. (I).

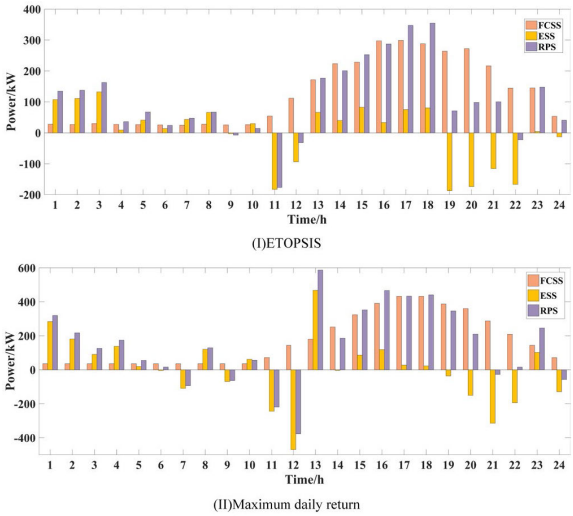


**FIGURE 13.** The output power of FCSS, ESS and regional power system. (I)Results of ETOPSIS; (II)Results of maximum daily return.

By combining Fig. 13 and Fig. 5, it can be observed that during off-peak hours when electricity prices are low, EV-IES purchases electricity from the RPS and stores it in the ESS to reduce electricity procurement costs. However, during peak hours when electricity prices are high, priority is given to meeting the operational needs of EV-IES. If the combined electricity generated by PV and ESS satisfies the operational needs of EV-IES, the surplus electricity is fed back to the RPS; otherwise, it reduces the amount of electricity purchased during high-price peak hours. This approach maximizes the daily revenue of EV-IES, reduces the peak-to-valley difference in electricity demand after EVs are connected to the grid, and minimizes the impact on the safety and stability of the RPS. In Fig. 13, the comparison between the optimal operational scheme and the maximum daily revenue scheme shows that the total electricity charged from ESS to RPS in the optimal operational scheme is less than in the maximum daily revenue scheme, thereby satisfying the objective function of minimizing pollutant emissions.

From Fig. 13. (I), it can be seen that the ESS is in a discharged state during eight time periods (9, 11-12, 19-22, 24), while in the remaining time periods, the energy in the ESS is provided by PV and RPS. During four time periods (9, 11, 12, 22), the entire system feeds back electricity to the RPS, and the RPS provides energy to the ESS or the FCSS during the remaining time periods. At the same time, when the ESS is charging, the PV output prioritizes meeting the energy needs of the FCSS and ESS, with any surplus energy being fed back to the RPS. When the ESS is discharging, the optimization of PV system output meets the energy needs of the FCSS. If there is excess energy, it is fed back to the RPS. If the energy is insufficient to meet the FCSS requirements, the remaining energy is provided by the RPS.

It is evident from the time periods of ESS discharge and when EV-IES feeds back electricity to the RPS that these periods fall within high electricity price hours, while the ESS charging periods correspond to non-peak electricity price hours. This helps reduce electricity procurement costs, increase economic returns during high-price hours, and maximize the revenue of EV-IES.

In summary, by comparing the emissions of pollutants for each scenario, as shown in Fig. 14, it can be observed that case 4 has the lowest total emissions of pollutants. Additionally, the daily revenue of the EV-IES is also the highest among the four cases, with a value of 2536.33 yuan. Furthermore, it can be seen that in the traditional case (case 1), the pollutant emissions in each period are greater than zero, while in case 2, pollutant emissions are zero in the 10th and 11th time periods. In case 3, pollutant emissions are zero in the 11th and 12th time periods, and in case 4, pollutant emissions are zero in the 9th, 11th, 12th, and 22nd time periods. Moreover, in cases 3 and 4, pollutant emissions during the low-price electricity periods are significantly higher than in cases 1 and 2, while during the high-price electricity periods, pollutant emissions in cases 3 and 4 are significantly lower than in cases 1 and 2. This phenomenon is a result of the intervention of PV and ESS. The PV reduces the EV-IES of purchased electricity from the RPS, thereby increasing daily revenue, reducing pollutant emissions, and decreasing energy exchange between the RPS and the EV-IES. The ESS purchases electricity during low-price electricity periods and sells electricity or

reduces electricity purchases during high-price electricity periods, further increasing daily revenue for the EV-IES.

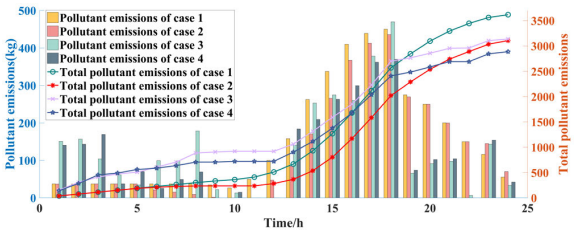


**FIGURE 14.** Pollutant emissions and total pollutant emissions of the EV-IES for each period in each case.

## VI. CONCLUSION

In order to achieve energy conservation and emission reduction, the widespread adoption of EVs is considered an important means. However, directly connecting a large number of EVs to the grid can increase the charging load on the RPS, which may affect the stability and safe operation of the system. Therefore, this paper designs an EV-IES that includes a PV system, an ESS, and an FCSS. It optimizes three objectives: maximizing the daily revenue of the EV-IES, minimizing the energy exchange between the RPS and the EV-IES, and minimizing pollutant emissions. Additionally, a MOSCO algorithm is proposed and validated through both benchmark functions and model-based approaches. Furthermore, three comparative cases are designed, and the proposed EV-IES model increases daily revenue by 27.97% and reduces pollutant emissions by 25.29% compared to traditional charging stations (Case 1). This study validates the feasibility of the EV-IES model, with future work focusing on addressing ESS battery losses.

## ACKNOWLEDGMENT

The authors thank the help of the editor and reviewers.

## REFERENCES

[1] M. R. Sarker, H. Pandžic, and M. A. Ortega-Vazquez, "Optimal operation and services scheduling for an electric vehicle battery swapping station," *IEEE Trans. Power Syst.*, vol. 30, no. 2, pp. 901–910, Mar. 2015.

[2] J. Yang, W. Liu, K. Ma, Z. Yue, A. Zhu, and S. Guo, "An optimal battery allocation model for battery swapping station of electric vehicles," *Energy*, vol. 272, Jun. 2023, Art. no. 127109.

[3] S. Zhang, X. Li, Y. Li, Y. Zheng, and J. Liu, "A green-fitting dispatching model of station cluster for battery swapping under charging-discharging mode," *Energy*, vol. 276, Aug. 2023, Art. no. 127600.

[4] S. Li, W. Hu, D. Cao, T. Dragicevic, Q. Huang, Z. Chen, and F. Blaabjerg, "Electric vehicle charging management based on deep reinforcement learning," *J. Mod. Power Syst. Clean Energy*, vol. 10, no. 3, pp. 719–730, May 2022.

[5] Q. Kang, J. Wang, M. Zhou, and A. C. Ammari, "Centralized charging strategy and scheduling algorithm for electric vehicles under a battery swapping scenario," *IEEE Trans. Intell. Transp. Syst.*, vol. 17, no. 3, pp. 659–669, Mar. 2016.

[6] X. Zhao, Y. Yang, M. Qin, and Q. Xu, "Day-ahead dispatch of novel battery charging and swapping station based on distributionally robust optimization," *J. Energy Storage*, vol. 63, Jul. 2023, Art. no. 107080.

[7] Z. Moghaddam, I. Ahmad, D. Habibi, and Q. V. Phung, "Smart charging strategy for electric vehicle charging stations," *IEEE Trans. Transport. Electrific.*, vol. 4, no. 1, pp. 76–88, Mar. 2018.

[8] G. Wang, Z. Xu, F. Wen, and K. P. Wong, "Traffic-constrained multiobjective planning of electric-vehicle charging stations," *IEEE Trans. Power Del.*, vol. 28, no. 4, pp. 2363–2372, Oct. 2013.

[9] C. Li, N. Wang, W. Li, Q. Yi, and D. Qi, "A battery centralized scheduling strategy for battery swapping of electric vehicles," *J. Energy Storage*, vol. 51, Jul. 2022, Art. no. 104327.

[10] V. C. Onishi, C. H. Antunes, and J. P. F. Trovão, "Optimal energy and reserve market management in renewable microgrid-PEVs parking lot systems: V2G, demand response and sustainability costs," *Energies*, vol. 13, no. 8, p. 1884, Apr. 2020.

[11] A. Sangswang and M. Konghirun, "Optimal strategies in home energy management system integrating solar power, energy storage, and vehicle-to-grid for grid support and energy efficiency," *IEEE Trans. Ind. Appl.*, vol. 56, no. 5, pp. 5716–5728, Sep. 2020.

[12] S. Baik, Y. Jin, and Y. Yoon, "Determining equipment capacity of electric vehicle charging station operator for profit maximization," *Energies*, vol. 11, no. 9, p. 2301, Sep. 2018.

[13] G. K. Zaher, M. F. Shaaban, M. Mokhtar, and H. H. Zeineldin, "Optimal operation of battery exchange stations for electric vehicles," *Electr. Power Syst. Res.*, vol. 192, Mar. 2021, Art. no. 106935.

[14] Q. Xing, M. Cheng, S. Liu, Q. Xiang, H. Xie, and T. Chen, "Multi-objective optimization and dispatch of distributed energy resources for renewable power utilization considering time-of-use tariff," *Frontiers Energy Res.*, vol. 9, Apr. 2021, Art. no. 647199.

[15] X. Zhao, Y. Yang, M. Qin, and Q. Xu, "Multi-objective optimization of distribution network considering battery charging and swapping station," *Energy Rep.*, vol. 9, pp. 1282–1290, Oct. 2023.

[16] W. Zhang, A. Maleki, M. A. Rosen, and J. Liu, "Sizing a stand-alone solar-wind-hydrogen energy system using weather forecasting and a hybrid search optimization algorithm," *Energy Convers. Manage.*, vol. 180, pp. 609–621, Jan. 2019.

[17] X. Bai, Z. Wang, L. Zou, H. Liu, Q. Sun, and F. E. Alsaadi, "Electric vehicle charging station planning with dynamic prediction of elastic charging demand: A hybrid particle swarm optimization algorithm," *Complex Intell. Syst.*, vol. 8, no. 2, pp. 1035–1046, Apr. 2022.

[18] W. Yao, J. Zhao, F. Wen, Z. Dong, Y. Xue, Y. Xu, and K. Meng, "A multi-objective collaborative planning strategy for integrated power distribution and electric vehicle charging systems," *IEEE Trans. Power Syst.*, vol. 29, no. 4, pp. 1811–1821, Jul. 2014.

[19] B. Sun, "A multi-objective optimization model for fast electric vehicle charging stations with wind, PV power and energy storage," *J. Cleaner Prod.*, vol. 288, Mar. 2021, Art. no. 125564.

[20] R. Wang, J. Mu, Z. Sun, J. Wang, and A. Hu, "NSGA-II multi-objective optimization regional electricity price model for electric vehicle charging based on travel law," *Energy Rep.*, vol. 7, pp. 1495–1503, Nov. 2021.

[21] Y. Li, Y. Cai, T. Zhao, Y. Liu, J. Wang, L. Wu, and Y. Zhao, "Multi-objective optimal operation of centralized battery swap charging system with photovoltaic," *J. Mod. Power Syst. Clean Energy*, vol. 10, no. 1, pp. 149–162, Jan. 2022.

[22] L. Wang, Y. Wan, W. Cao, and Y. Cao, "Multi-objective orderly charging strategy for electric vehicles based on interactive network model," *IEEJ Trans. Electr. Electron. Eng.*, vol. 16, no. 4, pp. 519–525, Apr. 2021.

[23] R. Das, Y. Wang, G. Putrus, R. Kotter, M. Marzband, B. Herteleer, and J. Warmerdam, "Multi-objective techno-economic-environmental optimisation of electric vehicle for energy services," *Appl. Energy*, vol. 257, Jan. 2020, Art. no. 113965.

[24] H. H. Eldeeb, S. Faddel, and O. A. Mohammed, "Multi-objective optimization technique for the operation of grid tied PV powered EV charging station," *Electr. Power Syst. Res.*, vol. 164, pp. 201–211, Nov. 2018.

[25] S. Shi, C. Fang, H. Wang, J. Li, Y. Li, D. Peng, and H. Zhao, "Two-step intelligent control for a green flexible EV energy supply station oriented to dual carbon targets," *Processes*, vol. 9, no. 11, p. 1918, Oct. 2021.

[26] J. A. Domínguez-Navarro, R. Dufo-López, J. M. Yusta-Loyo, J. S. Artal-Sevil, and J. L. Bernal-Agustín, "Design of an electric vehicle fast-charging station with integration of renewable energy and storage systems," *Int. J. Electr. Power Energy Syst.*, vol. 105, pp. 46–58, Feb. 2019.

[27] Y. Zheng, S. Xie, Z. Hu, J. Wang, and S. Kong, "The optimal configuration planning of energy hubs in urban integrated energy system using a two-layered optimization method," *Int. J. Electr. Power Energy Syst.*, vol. 123, Dec. 2020, Art. no. 106257.

[28] F. Wei, Q. H. Wu, Z. X. Jing, J. J. Chen, and X. X. Zhou, "Optimal unit sizing for small-scale integrated energy systems using multi-objective interval optimization and evidential reasoning approach," *Energy*, vol. 111, pp. 933–946, Sep. 2016.
[29] H. Miao, H. Jia, J. Li, and T. Z. Qiu, "Autonomous connected electric vehicle (ACEV)-based car-sharing system modeling and optimal planning: A unified two-stage multi-objective optimization methodology," *Energy*, vol. 169, pp. 797–818, Feb. 2019.
[30] F. Xu, J. Liu, S. Lin, Q. Dai, and C. Li, "A multi-objective optimization model of hybrid energy storage system for non-grid-connected wind power: A case study in China," *Energy*, vol. 163, pp. 585–603, Nov. 2018.
[31] J. Sarshar, S. S. Moosapour, and M. Joorabian, "Multi-objective energy management of a micro-grid considering uncertainty in wind power forecasting," *Energy*, vol. 139, pp. 680–693, Nov. 2017.
[32] M. H. Amrollahi and S. M. T. Bathaee, "Techno-economic optimization of hybrid photovoltaic/wind generation together with energy storage system in a stand-alone micro-grid subjected to demand response," *Appl. Energy*, vol. 202, pp. 66–77, Sep. 2017.
[33] V. Hayyolalam and A. A. P. Kazem, "Black widow optimization algorithm: A novel meta-heuristic approach for solving engineering optimization problems," *Eng. Appl. Artif. Intell.*, vol. 87, Jan. 2020, Art. no. 103249.
[34] F. A. Hashim and A. G. Hussien, "Snake optimizer: A novel meta-heuristic optimization algorithm," *Knowledge-Based Syst.*, vol. 242, Apr. 2022, Art. no. 108320.
[35] H.-C. Liu, L.-E. Wang, Z. Li, and Y.-P. Hu, "Improving risk evaluation in FMEA with cloud model and hierarchical TOPSIS method," *IEEE Trans. Fuzzy Syst.*, vol. 27, no. 1, pp. 84–95, Jan. 2019.
[36] D.-F. Li, "TOPSIS-based nonlinear-programming methodology for multiattribute decision making with interval-valued intuitionistic fuzzy sets," *IEEE Trans. Fuzzy Syst.*, vol. 18, no. 2, pp. 299–311, Apr. 2010.
[37] E. K. Zavadskas, A. Mardani, Z. Turskis, A. Jusoh, and K. M. Nor, "Development of TOPSIS method to solve complicated decision-making problems—An overview on developments from 2000 to 2015," *Int. J. Inf. Technol. Decis. Making*, vol. 15, no. 3, pp. 645–682, May 2016.
[38] P. Chen, "Effects of the entropy weight on TOPSIS," *Expert Syst. Appl.*, vol. 168, Apr. 2021, Art. no. 114186.
[39] W. Huang, B. Shuai, Y. Sun, Y. Wang, and E. Antwi, "Using entropy-TOPSIS method to evaluate urban rail transit system operation performance: The China case," *Transp. Res. A, Policy Pract.*, vol. 111, pp. 292–303, May 2018.
[40] Y.-N. Wang, L.-H. Wu, and X.-F. Yuan, "Multi-objective self-adaptive differential evolution with elitist archive and crowding entropy-based diversity measure," *Soft Comput.*, vol. 14, no. 3, pp. 193–209, Feb. 2010.
[41] E. Zitzler and L. Thiele, "Multiobjective evolutionary algorithms: A comparative case study and the strength Pareto approach," *IEEE Trans. Evol. Comput.*, vol. 3, no. 4, pp. 257–271, Nov. 1999.
[42] D. Gong, J. Sun, and Z. Miao, "A set-based genetic algorithm for interval many-objective optimization problems," *IEEE Trans. Evol. Comput.*, vol. 22, no. 1, pp. 47–60, Feb. 2018.
[43] M. Li and X. Yao, "Quality evaluation of solution sets in multiobjective optimisation: A survey," *ACM Comput. Surv.*, vol. 52, no. 2, pp. 1–38, Mar. 2020.
[44] Z. Liu, Y. Chen, R. Zhuo, and H. Jia, "Energy storage capacity optimization for autonomy microgrid considering CHP and EV scheduling," *Appl. Energy*, vol. 210, pp. 1113–1125, Jan. 2018.
[45] G. Liu, L. Kang, Z. Luan, J. Qiu, and F. Zheng, "Charging station and power network planning for integrated electric vehicles (EVs)," *Energies*, vol. 12, no. 13, p. 2595, Jul. 2019.
[46] K. Deb and H. Jain, "An evolutionary many-objective optimization algorithm using reference-point-based nondominated sorting approach: Solving problems with box constraints," *IEEE Trans. Evol. Comput.*, vol. 18, no. 4, pp. 577–601, Aug. 2014.
[47] Q. Cheng, B. Du, L. Zhang, and R. Liu, "ANSGA-III: A multiobjective endmember extraction algorithm for hyperspectral images," *IEEE J. Sel. Topics Appl. Earth Observ. Remote Sens.*, vol. 12, no. 2, pp. 700–721, Feb. 2019.
[48] H. Zille, H. Ishibuchi, S. Mostaghim, and Y. Nojima, "Mutation operators based on variable grouping for multi-objective large-scale optimization," in *Proc. IEEE Symp. Ser. Comput. Intell. (SSCI)*, Dec. 2016, pp. 1–8.
[49] Y. Yuan, H. Xu, B. Wang, and X. Yao, "A new dominance relation-based evolutionary algorithm for many-objective optimization," *IEEE Trans. Evol. Comput.*, vol. 20, no. 1, pp. 16–37, Feb. 2016.
[50] K. Deb, A. Pratap, S. Agarwal, and T. Meyarivan, "A fast and elitist multiobjective genetic algorithm: NSGA-II," *IEEE Trans. Evol. Comput.*, vol. 6, no. 2, pp. 182–197, Apr. 2002.

**BANGLI YIN** received the bachelor's degree in mechanical and electronic engineering from the Hunan Institute of Technology, in 2021. He is currently pursuing the master's degree in electrical engineering with the Hubei University of Technology. His research interests include multi-energy system optimization control and intelligent optimization methods.

**XIANG LIAO** received the Ph.D. degree in science from the Huazhong University of Science and Technology. He completed a postdoctoral program in hydraulic engineering. He is an Associate Professor and the Master's Supervisor at the School of Electrical and Electronic Engineering, Hubei University of Technology. He has led three scientific research projects, including the National Natural Science Foundation Youth Project and the Postdoctoral Science Foundation Project. His research interests include multi-energy system optimization control, optimization scheduling of hydropower station groups, intelligent optimization methods, and forecasting and reporting technologies.

**BEIBEI QIAN** received the bachelor's degree in electrical engineering from the Hebei University of Science and Technology, in 2020, where he is currently pursuing the master's degree in electrical engineering. His research interests include multi-energy system optimization control and intelligent optimization methods.

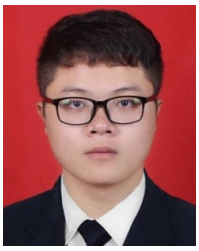

**JUN MA** received the bachelor's degree in electrical engineering and its automation from the Cunjin College, Guangdong Ocean University, in 2019. He is currently pursuing the master's degree in electrical engineering with the Hubei University of Technology. His research interests include multi-energy system optimization control and intelligent optimization methods.

**RUNJIE LEI** received the bachelor's degree in electrical engineering and its automation from the Hubei University of Technology, in 2021, where he is currently pursuing the master's degree in electrical engineering. His research interests include multi-energy system optimization control and intelligent optimization methods.